Resubmitted to *Icarus* journal

Yarkovsky effect on small near–Earth asteroids: Mathematical formulation and examples

D. Vokrouhlický

Institute of Astronomy, Charles University, V Holešovičkách 2, CZ–18000 Prague 8, Czech Republic

A. Milani

Dipartimento di Matematica, Università di Pisa, Via Buonarroti, I–56127 Pisa, Italy

S.R. Chesley

Jet Propulsion Laboratory, California Institute of Technology, Pasadena 91109, USA

ABSTRACT

The Yarkovsky effect is a subtle non–gravitational phenomenon related to the anisotropic thermal emission of solar system objects. Its importance has been recently demonstrated in relation to the transport of material from the main asteroid belt (both to explain the origin of near–Earth asteroids and some properties of meteorites) and also in relation to the aging processes of the asteroid families. However, unlike the case of the artificial satellites, the Yarkovsky effect has never been measured or detected in the motion of natural bodies in the solar system. In this paper, we investigate the possibility of detecting the Yarkovsky effect via precise orbit determination of near–Earth asteroids. Such a detection is feasible only with the existence of precise radar astrometry at multiple apparitions. Since the observability of the Yarkovsky perturbation accumulates quadratically with time the time span between radar observations is a critical factor. Though the current data do not clearly indicate the Yarkovsky effect in the motion of these bodies, we predict that the next apparition of several asteroids (in particular, 6489 Golevka, 1620 Geographos, and possibly 1566 Icarus) might reveal its existence. Moreover, we show that the Yarkovsky effect may play a very important role in the orbit determination of small, but still observable, bodies like 1998 KY_{26}. If carefully followed, this body may serve as a superb probe of the Yarkovsky effect in its next close approach to the Earth in June 2024.

Subject headings: asteroids, Yarkovsky effect, orbit determination

Editorial Correspondence and Proofs:

Steven Chesley
M/S 301-150
Jet Propulsion Laboratory
Pasadena, CA 91109

Phone: (818) 354-9615
Fax: (818) 393-6388
E-mail: steve.chesley@jpl.nasa.gov

1. Introduction and motivations

The orbital dynamics of near–Earth objects (NEOs) reveal many complex problems. Among them, the influence of close planetary encounters has been extensively studied and recognized to be a principal reason for their strong chaoticity and short dynamical lifetime. However, besides this short–range gravitational interaction with terrestrial planets there might be additional dynamical effects that increase the difficulty of modeling the NEO dynamics. The purpose of this paper is to analyze the influence on NEO motion of the Yarkovsky effect, a subtle non–gravitational perturbation due to a recoil force of anisotropically emitted thermal radiation of a rotating body. Since the perspective of our effort is to consider a possible observability of the Yarkovsky effect, we shall not investigate its role on the dynamical lifetime of NEO orbits nor its influence on very small NEOs (e.g., the meteorite precursors of a typical size 0.5 to 5 meters; see, e.g., Vokrouhlický and Farinella 2000). We rather restrict our analysis to understanding the orbital perturbation induced by the Yarkovsky effect for the presently observed near–Earth asteroids (NEAs). Obviously, the short time scale involved ($\simeq$ years) has to be compensated by very high precision observations. Fortunately, we have available the radar observations of about 50 NEAs, some of which have been observed with radar even during two apparitions. We intend to demonstrate that data of such a superb quality may reveal the influence of the Yarkovsky effect on several NEA orbits.

The plan of the paper is as follows: in Sec. 2 we briefly recall the physical essence of the Yarkovsky effect and discuss the mathematical approach that will be used. Though we basically put together previous results, new results presented in this paper include the definition of algorithms to determine the model parameters of the diurnal Yarkovsky acceleration (the surface thermal conductivity and the orientation of its spin axis). We shall also point out that modeling of the Yarkovsky effect on the NEA orbits presents a special problem not encountered in the similar orbital analysis of the main–belt objects, and that is their high eccentricity. Then, in Sec. 3, we determine the secular semimajor axis drift (the main orbit perturbation) caused by the Yarkovsky effect for selected known NEAs and we estimate, using simple analytical formulas, a characteristic orbital change produced by this effect. These results offer a first glimpse of a more complete understanding of the way the Yarkovsky effect affects NEA orbits. We shall also consider how the results depend on the value of the surface thermal conductivity of the asteroid, which is a particularly important issue in the context of this paper. However, the detection of the Yarkovsky effect via NEA observations and orbit determination requires also a detailed consideration of both observational and orbit determination errors. The observation errors are small enough to allow for the detection of the Yarkovsky effect, since the present precision of the radar ranging technology is on the level of a fraction of a μs or about 60 meters in range and about 100 meters/day in the range–rate measurement. However, the global orbit determination uncertainty must be considered, and it substantially excludes the possibility of detection of the non–gravitational perturbations within the currently available data. We then discuss which additional observations would be sufficient for this detection, and find some very interesting possibilities for the next few years. We devote Sec. 4 to this topic.

2. Yarkovsky effect: the split onto diurnal and seasonal variants

The applications of the Yarkovsky effect in solar system dynamics have undergone a remarkable renaissance over the last few years. This situation results from a fruitful conjunction of progress in several fields. On one side, the classical understanding of the Yarkovsky effect has been enlarged by a more detailed theoretical analysis that finally resulted in the recognition of the mean–motion mode of the thermal effect (now called the "seasonal" variant of the Yarkovsky effect; see, e.g., Rubincam 1995, 1998, Farinella *et al.* 1998 and below). On the observational side, direct and indirect knowledge of the dynamics of the small solar system bodies has dramatically increased during the last few years. Here we have in mind the systematic searches for NEOs with the powerful CCD systems, the previously mentioned radar ranging to NEAs and also more detailed and precise measurements of the cosmic–ray exposure ages of meteorites (that provide an indirect evidence for the transfer time from the main asteroid belt toward the Earth; e.g., Graf and Marti 1995, Herzog *et al.* 1997).

Though the role of Yarkovsky perturbation has been recently discussed in relation to meteorite properties (e.g., Farinella *et al.* 1998; Hartmann *et al.* 1999; Vokrouhlický and Farinella 2000; Bottke *et al.* 2000), the replenishment of large NEAs (e.g., Farinella and Vokrouhlický 1999) and asteroid family aging processes (e.g., Farinella and Vokrouhlický 1999; Vokrouhlický *et al.* 2000), so far there has not been any direct measurement of the Yarkovsky perturbation in the orbital motion of the natural bodies in the solar system (despite extensive *observational* evidence of the Yarkovsky effect in the case of a motion of artificial Earth satellites such as LAGEOS, e.g., Rubincam 1987). Though the Yarkovsky effect is unavoidable from the perspective of physical principles, its direct measurement might validate the available (and necessarily approximate) models for the natural bodies like asteroids and their fragments. In this way it would also enhance the credibility of the other ongoing work related to the Yarkovsky effect. This line of thinking is a principal motivation of the present work.

It is also worth mentioning that the orbit analysis of some NEAs has suggested the evidence of non–gravitational phenomena by requiring an anomalous secular decrease of their semimajor axis (e.g., Sitarski 1992, 1998). At that stage of analysis no precise physical mechanism was mentioned apart from a possible, but vague, reference to outgassing, comet–like processes (conformal to the usage of the classical empiric approach to model the non–gravitational effects on cometary orbits: $\mathbf{a}_{\rm pert} \simeq (\dot{a}/2a)\,\mathbf{v}$; Sitarski 1998). Involving the Yarkovsky effect in the orbit analysis of these cases might offer an additional and perhaps more sophisticated approach.

As mentioned above, the Yarkovsky effect is a recoil force from the thermal radiation of cosmic bodies that accumulate the energy by absorption of the solar radiation in the optical band. As a result, an anisotropic distribution of the surface temperature is a necessary condition for a nonzero Yarkovsky force. For a given surface element of the body, the incoming solar radiation flux in the body–fixed reference frame is essentially modulated by two frequencies: (i) the rotation frequency of the body around an instantaneous spin axis and (ii) the mean motion frequency that is given by the body's revolution around the Sun (plus their multiples and linear combinations). In the context of a simple (linearized) heat diffusion theory the temperature variation of the surface element basically keeps the same spectral characteristic with one exception: the individual spectral lines are phase–shifted in a precisely determined way. When performing the inverse Fourier map these phase–shifts obviously then appear as time–lags. Taking into account the assumed spherical geometry of the body and the individual temperature history of the surface elements, computed according to the above–mentioned theory, we may determine the net recoil force of the thermal radiation (by performing a surface integration of the infinitesimal effects on the sphere).

The theoretical re–analysis of the Yarkovsky effect over the last few years (e.g., Rubincam 1995, 1998; Farinella *et al.* 1998; Vokrouhlický 1998a,b, 1999) has revealed the following important results. The surface–integrated Yarkovsky acceleration terms that depend on the rotation frequency of the body are tightly clustered around the spectral line with this frequency (showing–up as mean–motion sidebands) and yield acceleration components perpendicular to the spin axis. Thanks to the typically big difference between the periods of rotation ($\approx$ hours) and revolution ($\approx$ years), these acceleration terms in practice "collapse" to the single spectral line corresponding simply to the rotation frequency. The other aspect of the same reasoning comes from the fact that the thermal relaxation time scale corresponding to the rotation frequency of the body (approximately the time between the sunlight absorption and the thermal emission) is comparable to the rotation period and thus the body's shift along the orbit around the Sun may be neglected. When these force components are transformed to the inertial reference frame, to which the orbital perturbations are referred, they have close to zero frequency with amplitude still depending on the rotation rate of the body. Because of their relation to the rotation period the above–mentioned acceleration terms are usually called "diurnal". Their modeling is sufficiently simple since they depend uniquely on the instantaneous state vector of the body on its orbit. In particular, the eccentricity of the orbit does not enter the computation of the diurnal Yarkovsky acceleration components at this level of approximation. However, in his pioneering work, Rubincam (1995; but see also his related work in satellite dynamics, Rubincam 1987) has shown that there exists another class of thermal acceleration terms, computed by the surface integration mentioned in the previous paragraph, that do not depend on the rotation frequency of the body but only on its revolution frequency around the Sun (and its multiples). These terms, usually called "seasonal" because of their frequency characteristics, are always aligned with the body's spin axis. Since we assume a fixed orientation of the spin axis in the inertial space, the seasonal component of the Yarkovsky force preserves its revolution frequency even in the inertial frame. If described in an approximate way, the seasonal acceleration terms are related to the changing geometry of the north/south hemisphere insolation of the body. Each of these two effects, diurnal and seasonal, may be important in the dynamics of small cosmic bodies like NEAs.

Keeping the terminological and practical split into the above–mentioned diurnal and seasonal variants of the Yarkovsky effect, we shall summarize our mathematical approach in the remainder of this section. In the case of the diurnal variant we shall essentially follow the approach developed by

Vokrouhlický (1998a). The necessary formulas are given in Sec. 2.1 and the partials with respect to the most important parameters are computed analytically. The seasonal variant of the Yarkovsky effect deserves more attention since it hides more complicated problems. The latter arise mainly because of high orbital eccentricities (that can range from 0.3 up to very "extreme", cometary–like values; e.g., $\simeq 0.823$ in the case of 1566 Icarus), so that the analytic evaluation of the incoming solar radiation flux becomes troublesome. On top of this difficulty, Vokrouhlický and Farinella (1998) have pointed out another problem in evaluating the seasonal component of the thermal force. For the highly eccentric orbits the variations of temperature along the orbit, in particular over a thermal relaxation time scale of the seasonal effect, are large enough so that the basic assumptions of linearization of the heat diffusion problem are violated. Avoiding the linearization approach yields a precise result, but requires a completely numerical solution. In what follows, we shall use the model of Vokrouhlický and Farinella (1998) that solves the thermal state of the body along an arbitrarily eccentric orbit in the "large–body" approximation (penetration depth of the seasonal thermal wave much smaller than the geometric size of the body). The amplitude of the seasonal Yarkovsky acceleration is then formally given in terms of an integral in which the integrand contains the latitude stratification of the surface temperature. The latter, in turn, results from a solution of a partial differential heat–diffusion equation. The corresponding formulas are outlined in Sec. 2.2.2. Though precise, this model for the seasonal Yarkovsky force may not be well suited for the routine orbit determination process because of its complexity. We thus also consider a less precise, but analytical solution by Vokrouhlický and Farinella (1999), which is based on linearization of the heat diffusion problem. The corresponding formulas are outlined in Sec. 2.2.1.

2.1. Yarkovsky diurnal acceleration

There are two basic assumptions of the Vokrouhlický (1998a) model of the diurnal variant of the Yarkovsky effect: (i) temperature throughout the body is close to a mean value, and (ii) the body is spherical (with radius R). The first of these two items allows linearization of the heat diffusion problem and, thus, analyticity of the solution. Since the thermal relaxation time, estimated above, is not much shorter than the rotation period, the item (i) might be a fairly good approximation. The second item (ii) might present an obstacle for small NEAs, since they are usually of a rather irregular shape (e.g., Ostro *et al.* 1996, 1999a for the most extreme cases of 1620 Geographos and 4179 Toutatis; some are fortunately less elongated objects, like 1566 Icarus with the following ratio of the dimension along the inertia–moment principal axes $a/b = 1.23 \pm 0.04$ and $b/c = 1.40 \pm 0.10$, e.g., De Angelis 1995). Vokrouhlický (1998b) has developed a theory for computing the diurnal Yarkovsky acceleration on spheroidal objects (whose size is much larger than the penetration depth of the diurnal thermal wave), but his results are not easily incorporated into numerical integrations, especially for the nonprincipal–axis–rotators; moreover, their generalization for triaxial bodies would only increase the complexity. Given the substantial uncertainty in our knowledge of the surface thermal parameters, we believe that errors incurred by the use of the spherical assumption may be partly aliased into the estimation of the surface conductivity (or the effective size of the body). Tailoring the thermal model for a given shape of an asteroid (as is typical in the case of artificial satellites) will probably turn out to be necessary in the future, but this topic is beyond the scope of this paper.

The diurnal variant of the Yarkovsky acceleration can be written in the following form (see also Brož *et al.* 2000)

$$\mathbf{a}_{\rm d} = \frac{4\alpha}{9}\,\frac{\Phi(r)}{1+\lambda}\,G\,\left[\sin\delta + \cos\delta\,\mathbf{s}\times\right]\,\frac{\mathbf{r}\times\mathbf{s}}{r}\;, \tag{1}$$

where α is the absorptivity of the asteroid surface in the optical band (complementary to albedo), $\mathbf{s}$ is the unit vector of the spin axis and $\mathbf{r}$ is the heliocentric position vector ($r = |\mathbf{r}|$). The standard radiation force–factor Φ is defined by

$$\Phi(r) = \frac{3F(r)}{4R\rho c}\;, \tag{2}$$

with $F(r)$ being the solar radiation flux at the instantaneous distance r from the Sun [hence $F(r) \propto 1/r^2$], c is the speed of light and ρ the mean density of the fragment. The instantaneous solar radiation flux $F(r)$ determines the local (in terms of the orbital revolution) subsolar temperature $T(r)$ through

$$\epsilon\sigma T^4(r) = \alpha F(r)\;, \tag{3}$$

with σ being the Stefan–Boltzmann constant. The subsolar temperature defines the diurnal thermal parameter $\Theta = \sqrt{K\rho_{\rm s}C\omega}/\epsilon\sigma T^3(r)$ and the local value of the penetration depth of the diurnal thermal wave $l_{\rm d} = \sqrt{K/\rho_{\rm s}C\omega}$. Here K is the thermal conductivity, C the thermal capacity, ω is the rotation frequency and $\rho_{\rm s}$ is the surface density. In principle, this latter quantity may not be identical to the mean bulk density ρ from Eq. (2). The argument X in Eq. (4) is $X = \sqrt{2}\,R/l_{\rm d}$ and the parameter λ is defined by $\lambda = \Theta/X$.

Finally, the amplitude G and the phase δ in Eq. (1) are given by

$$G e^{i\delta} = \frac{A(X) + iB(X)}{C(X) + iD(X)}\;, \tag{4}$$

($i = \sqrt{-1}$ is the complex unit) with the auxiliary functions

$$\begin{aligned}
A(x) &= -(x+2) - e^x\left[(x-2)\cos x - x\sin x\right]\;, && (5)\\
B(x) &= -x - e^x\left[x\cos x + (x-2)\sin x\right]\;, && (6)\\
C(x) &= A(x) + \frac{\lambda}{1+\lambda}\Big\{3\,(x+2) + e^x[3(x-2)\cos x + x\,(x-3)\sin x]\Big\}\;, && (7)\\
D(x) &= B(x) + \frac{\lambda}{1+\lambda}\Big\{x\,(x+3) - e^x[x(x-3)\cos x - 3\,(x-2)\sin x]\Big\}\;. && (8)
\end{aligned}$$

A few remarks are in order to illuminate the features of the diurnal acceleration (1).

- Notice, that the diurnal acceleration (1) is perpendicular to the body's spin axis ($\mathbf{a}_{\rm d} \cdot \mathbf{s} = 0$). The along–spin acceleration component is then given by the seasonal variant of the Yarkovsky effect and it will be discussed below.

- For future use we introduce functions $a(x)$ and $b(x)$ by the following formulas: $C(x) = A(x) + \frac{\lambda}{1+\lambda} a(x)$ and $D(x) = B(x) + \frac{\lambda}{1+\lambda} b(x)$.

- As a reference check of the numerical simulations, we mention here the analytical estimation of the semimajor axis drift due to the diurnal variant of the Yarkovsky effect (e.g., Vokrouhlický 1998a, 1999)

$$\frac{da}{dt} = -\frac{8\alpha}{9n}\, \Phi(a)\, \frac{G\, \sin\delta}{1+\lambda}\, \cos\gamma + \mathcal{O}(e). \tag{9}$$

  [$\Phi(a) = \Phi(r = a)$ since (9) is correct for the circular orbit only]. Here, n is the mean motion and γ is the obliquity of the body's spin axis. Numerical tests indicate that for high eccentricity orbits (like 1566 Icarus, $e \simeq 0.827$) the approximate result (9) should be increased by a factor of $1 - 5$.

Some of the Yarkovsky effect parameters might be adjusted in the orbit determination procedure. For this goal we would need to calculate partial derivatives of the diurnal Yarkovsky acceleration (1) with respect to those parameters. Some of them are given below.

Since the surface thermal conductivity K is the principal unknown parameter of the thermal model outlined above, the orbit determination should focus on fitting this parameter. Anticipating the results of this paper, we note that the NEA orbits/objects can have either a weak or a strong dependence of the resulting orbital perturbations on the surface conductivity K. Both cases can be interesting. In the first case the results do not depend on a badly constrained parameter in the model, while in the second case we might wish to determine, or at least constrain, the surface conductivity value. We recall that the knowledge of the latter might have impose constraints on the physical character of the surface (degree of particularization, existence of regolith etc.) that, in turn, has cosmogonic implications.

The corresponding partial derivative of the diurnal Yarkovsky acceleration (1) is

$$K\,\partial_K\,\left(\mathbf{a}_{\rm d}\right) = \frac{4\alpha}{9}\,\Phi(r)\left\{K\,\partial_K\left(\frac{G\sin\delta}{1+\lambda}\right) + K\,\partial_K\left(\frac{G\cos\delta}{1+\lambda}\right)\mathbf{s}\times\right\}\frac{\mathbf{r}\times\mathbf{s}}{r} \tag{10}$$

($\partial_K = \partial/\partial K$). The partial derivatives at the right hand side can be determined from the following relation

$$K\,\partial_K\left\{\frac{G\exp i\delta}{1+\lambda}\right\} = -\frac{G\exp i\delta}{1+\lambda}\,\xi_K\ , \tag{11}$$

where the complex factor ξ_K is given by

$$\xi_K = \frac{\lambda}{1+\lambda}\left\{1 + \frac{X}{2}\,\frac{[A'(X)+iB'(X)]\,[a(X)+ib(X)] - [A(X)+iB(X)]\,[a'(X)+ib'(X)]}{[A(X)+iB(X)]\,[C(X)+iD(X)]}\right\}\ . \tag{12}$$

Here we have used with respect to their argument reading

$$A'(x) = \frac{dA(x)}{dx} = -1 + e^x \left[\cos x + (2x-1)\sin x\right] \ , \tag{13}$$

$$B'(x) = \frac{dB(x)}{dx} = -1 - e^x \left[(2x-1)\cos x - \sin x\right] \ , \tag{14}$$

$$a'(x) = \frac{da(x)}{dx} = 3 + e^x \left[\left(x^2-3\right)\cos x + \left(x^2-4x+3\right)\sin x\right] \ , \tag{15}$$

$$b'(x) = \frac{db(x)}{dx} = 2x + 3 - e^x \left[\left(x^2-4x+3\right)\cos x - \left(x^2-3\right)\sin x\right] \ . \tag{16}$$

In general, the thermal conductivity K, and to a lesser extent the thermal capacity C and the density ρ, are functions of the temperature. A higher mean temperature results in the melting the surface particles to a larger matrix that enables more efficient conduction, but decreases the role of the inter–grain radiation transport. Given such physical concepts of the heat transport in the surface material, several parametrizations of the K vs. T dependency were theoretically proposed and experimentally tested (e.g., Wesselink 1948, Glegg *et al.* 1966, Wechsler *et al.* 1972). However, given the other simplifications of our approach we shall neglect the temperature dependence of the thermal model parameters in this paper.

As mentioned above, the asteroids that we have selected in our study for a possible measurement of the Yarkovsky effect were all observed with radar technology. These were selected in order to obtain the highest precision of orbital data. Modern radar measurements allow the capability of determining both the orbit ("center–of–mass" position and motion) and the shape of the asteroid. This is, for instance, the case with 4179 Toutatis (Ostro *et al.* 1999a), 1620 Geographos (Ostro *et al.* 1996) and 6489 Golevka (Hudson *et al.* 2000). The objects are generally of a rather irregular shape, which is conventionally approximated by a triaxial ellipsoid. Since our model for the Yarkovsky force assumes a spherical body, we shall determine its effective radius R by an "equal–mass–condition": $R^3 = abc$, where a, b and c are radii along the principal axis of the ellipsoid model. In some other cases, however, we have much less reliable information about the size of the body. For instance Veeder *et al.* (1989) report the radius $R = 450$ meters for 1566 Icarus provided its albedo is about 0.4. This albedo, however, seems to be quite large, and Harris (1998) advocated a larger size for this asteroid and a correspondingly smaller optical albedo. In a recent paper, Mahapatra *et al.* (1999) however seem to indicate that the original solution of small–size Icarus might be correct. (This issue is carefully considered in Sec. 3.3.)

In these latter cases especially, it might be interesting to constrain the radius R of the body via the orbital perturbation of the Yarkovsky thermal effect. In other words, solving for the formal, Yarkovsky–determined radius of the body, we may also gain insight into the reliability of the Yarkovsky model for this particular body. To that end we need the partial derivatives of the Yarkovsky acceleration with respect to the radius of the body. The resulting formula is rather simple and, moreover, does not demand supplementary computational expense

$$R\,\partial_R\left(\mathbf{a}_{\rm d}\right) = -\frac{1+2\lambda}{1+\lambda}\,\mathbf{a}_{\rm d} - 2\,K\,\partial_K\left(\mathbf{a}_{\rm d}\right) \ , \tag{17}$$

where the derivative in the last right–hand–side term is given in (10) and was thus already computed. Obviously, both surface thermal conductivity K and the radius R of the body affect the semimajor axis change. Their simultaneous determination would not be possible. However, the situation might be interesting in several cases where the semimajor axis mobility depends little on the K value (see Sec. 3 below).

2.2. Yarkovsky seasonal acceleration

As explained above, the seasonal component of the thermal Yarkovsky acceleration is collinear with the orientation $\mathbf{s}$ of the spin axis, hence

$$\mathbf{a}_{\rm s} = f_Z \, \mathbf{s} \; . \tag{18}$$

Vokrouhlický (1999) obtained a simple analytic expression for f_Z which is, however, only valid for circular orbits, while Vokrouhlický and Farinella (1999) obtained a solution for the f_Z amplitude in terms of elliptic series that is formally valid for eccentric orbits. Both solutions are based on the linearization of the heat diffusion problem on a spherical body and, thus, cannot be fully precise. Obviously, the convergence of the elliptic–series solution of Vokrouhlický and Farinella (1999) is violated in the case of highly eccentric orbits (e.g., 1566 Icarus), so approximating the series by the first few terms, as we practically always have to do, may produce misleading results. The only precise approach then is a completely numerical solution. However, since this solution is computationally very difficult, we shall adopt two possible options for the seasonal Yarkovsky acceleration.

The first, "lower–precision" solution is based on the analytical results of Vokrouhlický and Farinella (1999). Our experience shows that it can be used up to eccentricity of 0.4–0.5 without a major corruption of the results. Its main advantage consists of its analyticity and thus high speed of numerical evaluation. For special cases of very eccentric orbits we shall use the "high–precision", numerical solution. Both approaches are briefly described in the following two paragraphs.

2.2.1. The low–precision model

At a lower precision of modeling the seasonal Yarkovsky effect we have adopted the linearized solution by Vokrouhlický and Farinella (1999). The acceleration amplitude f_Z from (18) then takes the following form (for more details see Brož *et al.* 2000)

$$f_Z = \frac{2\alpha}{9} \frac{\Phi(a)}{1+\lambda'} \sum_{k\neq 0} \chi_k G_k e^{i\delta_k} \zeta^k \; . \tag{19}$$

Here, $\lambda' = \lambda \, \eta^{3/4}$ ($\eta = \sqrt{1-e^2}$). In principle, the summation in (19) is to be performed over all integer and nonzero values of k; however, in our program we restrict to $|k| < 8$. This is justified for low–eccentricity orbits, since the χ_k factors decay fast with increasing value of the index k. In quantitative terms

$$\chi_k \equiv s_P \alpha_k - i s_Q \beta_k \propto e^{k-1} \; , \tag{20}$$

with e being the eccentricity. Obviously, the convergence of the series (19) is not guaranteed for high value of eccentricity. This is the principal caution behind using the lower–precision model for evaluation of the seasonal Yarkovsky acceleration.

Variables s_P and s_Q stand for projection of the spin vector $\mathbf{s}$ onto the orbit–defined unit vectors $\mathbf{P}$ (direction of pericenter; $s_P = \mathbf{s} \cdot \mathbf{P}$) and $\mathbf{Q} = \mathbf{N} \times \mathbf{P}$ (with $\mathbf{N}$ being normal to the orbit plane; $s_Q = \mathbf{s} \cdot \mathbf{Q}$). The eccentricity e dependent functions α_k and β_k read

$$\alpha_k = 2 \frac{d}{de} \left[J_k \left(ke \right) \right] \; , \tag{21}$$

$$\beta_k = 2 \frac{\eta}{e} \, k J_k \left(ke \right) \; , \tag{22}$$

where $J_k(x)$ are the ordinary Bessel functions of the first order. Explicit expressions of the first seven coefficients α_k and β_k can be found, for instance, in Brouwer and Clemence (1961).

The thermal characteristics of the seasonal effect are expressed by the amplitudes G_k and phases δ_k given by

$$G_k e^{i\delta_k} = \frac{A(X_k) + iB(X_k)}{C(X_k) + iD(X_k)} \; , \tag{23}$$

where we assume $k \geq 1$. Terms with the negative value of the index k are obtained by the identity $G_{-k} \exp i\delta_{-k} = G_k e^{-i\delta_k}$. The k-indexed arguments in the right hand side of (23) are $X_k = \sqrt{2k} R / l_{\rm s}$, with the radius R of the body scaled by the penetration depth $l_{\rm s}$ of the seasonal thermal wave $l_{\rm s} = \sqrt{K/\rho C n}$, and the functions A, B, C and D are defined by Eqs. (5) to (8) above. Finally, the complex quantity ζ in Eq. (19) denotes $\zeta = \exp i\ell$, where ℓ is the mean anomaly.

Notice that the structure of the acceleration (19) is very similar to that of the diurnal effect in (1). For an evaluation of the partial derivatives, with respect to the surface thermal conductivity (K) and the radius (R) of the body, we may straightforwardly use the formulas given in the previous section 2.1.1. Obviously, the seasonal effect related variables, e.g., scaling the radius of the body by the penetration depth of the seasonal thermal wave l_s, have to be used. In particular, the partial derivative of the f_Z–amplitude with respect to the surface conductivity K reads [compare with Eq. (10)]

$$K \, \partial_K \, \{ f_Z \} = - \frac{2\alpha}{9} \frac{\Phi(a)}{1+\lambda'} \sum_{k \neq 0} \chi_k \, G_k e^{i\delta_k} \, \xi^k_K \, \zeta^k \; . \tag{24}$$

where the complex factors ξ^k_K are

$$\xi^k_K = \frac{\lambda'}{1+\lambda'} \left\{ 1 + \frac{X_k}{2} \frac{\left[A'(X_k) \pm iB'(X_k) \right] \left[a(X_k) \pm ib(X_k) \right] - \left[A(X_k) \pm iB(X_k) \right] \left[a'(X_k) \pm ib'(X_k) \right]}{\left[A(X_k) \pm iB(X_k) \right] \left[C(X_k) \pm iD(X_k) \right]} \right\} \tag{25}$$

(the minus signs for negative values of the index k). Similarly the partial derivative with respect to the radius R of the body is given by

$$R\,\partial_R\,(\mathbf{a}_{\rm s}) = -\frac{1+2\lambda'}{1+\lambda'}\,\mathbf{a}_{\rm s} - 2\,K\,\partial_K\,(\mathbf{s}_{\rm s})\ , \tag{26}$$

which is identical (apart from the change $\lambda \to \lambda'$) to Eq. (17).

2.2.2. The high–precision model

In the case of orbits obeying a very high eccentricity, we shall use a non–linearized, fully numerical model developed by Vokrouhlický and Farinella (1998). Then, the amplitude f_Z from (18) is formally given as an integral over all latitudes θ on the body

$$f_Z = -\frac{4\alpha}{3}\Phi_a \int_{-1}^{1} d(\cos\theta)\,\cos\theta\,T'^4(\theta)\ , \tag{27}$$

with $\Phi_a = \pi R^2 F(a)/mc$ and $F(a)$ being the radiation flux at the semimajor axis distance from the center as before. The temperature T' in the integrand of (27) is scaled by the subsolar temperature at "the semimajor axis distance", i.e. $\epsilon\sigma T_{a,\star}^4 = \alpha F(a)$. Its latitudinal distribution $T'(\theta)$ results from a numerical solution of the 1–D heat diffusion equation with an appropriate boundary condition (see Vokrouhlický and Farinella 1998). Hence, our code first computes numerically $T'(\theta)$ at any instant along the orbit (of any eccentricity) and then computes f_Z by numerical quadrature (27).

Since the implementation of the "high–precision" seasonal Yarkovsky acceleration is completely numerical, we must also compute the partials by the finite difference method. To prevent numerical errors from computing the seasonal acceleration for two close values of the parameter for which we anticipate polynomial dependence (thermal conductivity K and radius R) we may use

$$\frac{\partial f_Z}{\partial K} = \frac{1}{K}\frac{\partial f_Z}{\partial \ln K} \tag{28}$$

and similarly for the radius R.

3. The first glimpse: semimajor axis mobility of NEAs and tests

In this section, we shall compute the expected drift of the semimajor axis for selected asteroids that might be the most promising candidates for determination of the Yarkovsky effect. Note, that the secular change of the semimajor axis is the principal indicator of the Yarkovsky orbital perturbation that can lead to observable effects (the perturbation of the other elements are less important except, perhaps, the inclination). As far as the "candidate bodies" are concerned we have selected the asteroids that had been observed by radar at two or more apparitions (according to the list given at `http://ssd.jpl.nasa.gov/radar_data.html`). These are generally the best known orbits among the NEAs. A list of the selected bodies is given in Table 1, where the assumed size and rotation parameters are also indicated. As far as the orbital parameters are concerned we used the `OrbFit` software, developed by the OrbFit Consortium (see `http://newton.dm.unipi.it/~asteroid/orbfit/`), which enables precise orbit determination (including radar observation processing). A check with the independent JPL solutions for individual objects has also been performed (e.g., Ostro *et al.* (1999a) for 4179 Toutatis). Since detailed information about the surface properties of these objects is usually not available, we shall span the surface thermal properties (in particular, the thermal conductivity K) in some physically reasonable range. The absorption coefficient α in the optical band is typically 0.9 (corresponding thus to albedo of 0.1), but in specific cases we accept the published values (e.g., the case of Icarus and Golevka). The emission coefficient ϵ in the thermal band is always set to 0.9.

The integrations performed in this section represent a perturbed two–body problem, i.e., no planetary effects have been included. This is already a fairly good approximation since we do not expect any significant coupling between the planetary and Yarkovsky perturbations. However, in Sec. 4 we shall proceed with a full numerical simulation involving a complete model for the orbit determination (including planetary perturbation and general relativity effects). We consider the effect of the diurnal and seasonal variants of the Yarkovsky effect separately. The total effect is then a simple superposition of the two variants at this level of approximation.

To understand how the computed drift in the semimajor axis translates into an orbital shift we perform the following estimate. The principal effect consists of a quadratic term in the asteroid anomaly of the order $\Delta M \simeq -\frac{3}{4}n(da/dt)(\Delta t)^2/a$ where n is the mean motion, da/dt the estimated semimajor axis drift due to the Yarkovsky effects, Δt the elapsed time between two observations and a the semimajor axis. This effect produces both transverse displacement $\Delta\tau \simeq a\eta\Delta M$ and a radial displacement $\Delta r \simeq ae\Delta M/\eta$ with $\eta = \sqrt{1-e^2}$ (see, e.g., Casotto 1992; notice that the radial displacement is to be dominated by the longitudinal term rather than by a change in the semimajor axis since the former effect is quadratic in time). The total displacement thus reads $\Delta\rho \simeq a\Delta M$, where the fourth–order terms in eccentricity have been neglected. In terms of physical units this means

$$\Delta\rho \simeq 7\, \dot{a}_4\, (\Delta_{10}t)^2\, a_{\rm AU}^{-3/2} \ \ {\rm km}\ , \qquad (29)$$

where $\dot{a}_4$ is the Yarkovsky drift of the semimajor axis in 10^{-4} AU/Myr (this is a typical order of magnitude of the Yarkovsky effects on the near–Earth objects; see below), $\Delta_{10}t$ is the time difference in tens of years (a characteristic temporal separation of two "radar apparitions") and $a_{\rm AU}$ is the semimajor axis in AU. We should mention that the actual displacement of the asteroid with respect to the radar station of the Earth then depends on a particular Earth–asteroid geometry. This effect may partly decrease the estimated value of $\Delta\rho$ from (29), though not by orders of magnitude. We shall check this claim in Sec. 4 where we shall perform a full numerical simulation of the objects displacement in their future apparitions. In the case of some NEAs we have a rather long series of optical observations (e.g., 1566 Icarus) or prediscovery identifications (e.g., 4179 Toutatis). Then,

Table 1: Candidate asteroids for detection of the Yarkovsky effect. For each of the objects we give: the semimajor axis a (in AU), radius R (in km), rotation period P (in hours), the ecliptic longitude and latitude (ℓ, b) of the spin axis orientation and its obliquity γ. The obliquity is helpful to get an idea of which of the variants of the Yarkovsky effect dominates; $\gamma \simeq 90^o$ means the seasonal variant is dominant, $\gamma \simeq 0(180)^o$ means the diurnal variant is dominant. Source references are listed in the last column.

Asteroid	a (AU)	R (km)	P (hr)	Spin axis orientation parameters [deg] ℓ	b	γ	Ref.
1566 Icarus [a]	1.08	0.45	2.273	214	5	103	1,2
1620 Geographos [b,c]	1.25	1.21	5.225	56	−47	150	3,4,5
1685 Toro	1.37	1.7	10.19	210	40	41	1,2
4179 Toutatis [b,d]	2.51	2.76	6.93	180	−52	143	4
6489 Golevka [b]	2.51	0.27	6.03	202	−45	134	6
1998 KY26 [e]	1.23	0.015	0.17837	–	–	0(180)?	7

[a] The quoted radius has been reported by Veeder *et al.* (1989). However, since these authors have used a rather high value of the albedo (0.4), the 0.45 km radius of 1566 Icarus may be just the lower estimate. In this context, notice the test we have performed in Sec. 3.3. For the spin axis orientation we use data by De Angelis (1995), whose analysis discarded the ambiguity in the sense of orientation of the Icarus spin axis.
[b] A triaxial model has been determined from radar observations, and we have estimated an "effective radius" by $R^3 \simeq abc$, where a, b and c are the dimensions along the principal axis of the moment of inertia.
[c] Spin axis orientation by Magnusson *et al.* (1997).
[d] We approximate the "spin axis orientation" by the direction along the angular momentum vector.
[e] This is one of the smallest objects observed so far by the radar technique. (Its smallness obviously favors the influence of the Yarkovsky effects.) The observations of 1998 KY_{26} might indicate the spin axis nearly perpendicular to the ecliptic plane (without possibility to resolve the sense of rotation; P. Pravec, personal communication).
REFERENCES.— (1) Veeder *et al.* (1989); (2) De Angelis (1995); (3) Ostro *et al.* (1996); (4) Ostro *et al.* (1999a); (5) Magnusson *et al.* (1997); (6) Hudson *et al.* (2000); (7) Ostro *et al.* (1999b).

we also express the longitude displacement ΔM directly:

$$\Delta M \simeq 0.01'' \, \dot{a}_4 \, (\Delta_{10} t)^2 \, a_{\rm AU}^{-5/2} \; . \qquad (30)$$

As the small NEAs are often observed at close approaches to the Earth only, this change in the mean anomaly may then imply a sky displacement (usually in the right ascension) given by $\Delta M \times (a/r_{\rm min})$, where $r_{\rm min}$ is the minimum distance to the Earth at the approach. The latter factor can sometimes result in a factor of 10–100 amplification of (30).

In what follows we shall assume the nominal estimates of the radii (given in Table 1). We have checked that the semimajor axis drift due to the Yarkovsky effects scales as $\propto R^{-1}$ for objects of sizes larger than about 20 meters (see, e.g., Farinella *et al.* 1998), a condition that applies for all the considered cases.

3.1. Diurnal Yarkovsky effect

In this section we shall deal with the diurnal variant of the Yarkovsky effect. Figure 1 shows the estimated values of the secular semimajor axis drift as a function of the surface conductivity K. If the surface is particularized (covered with the impact–produced regolith) or has a high degree of microporosity (due to the impacts of dust particles) its conductivity will be low: 0.001–0.01 W/m/K. On the other hand, if the body has a fresh, solid surface the conductivity would be significantly higher: $\simeq 1$ W/m/K. A lower degree of porosity of otherwise solid rock results in the thermal conductivity of about 0.1 W/m/K (e.g., Wechsler *et al.* 1972, Yomogida and Matsui 1983). This latter case is likely for very small objects such as 1998 KY$_{26}$ (radius of only 15 meters), while a value of 0.01 W/m/K seems the most likely value for the larger objects in our sample. Notice, that Müller *et al.* (1999) report typically very low values of the surface thermal conductivity ($\simeq 0.001$ W/m/K in our units) for the large main–belt asteroids from the thermophysical processing of the ISO measurements. This would indicate that these objects have regolith like surfaces. It seems reasonable to assume that the NEA surfaces (smaller and presumably younger objects) might have about a factor 10 times higher thermal conductivity as mentioned above.

We note that the diurnal effect may result in both semimajor axis increase and decrease, depending on the obliquity of the spin axis. In one case (1685 Toro) we have found da/dt positive (dashed line in Fig. 1), while in all other cases da/dt is negative (solid lines in Fig. 1). In the former case the contribution of the seasonal Yarkovsky effect may partially cancel the diurnal drift, while in the latter case it adds to the diurnal value.

The results in Fig. 1 indicate that a few parts in 10^4 (AU/Myr) are the typical values of the semimajor axis drift due to the diurnal variant of the Yarkovsky effect on our sample of bodies. This order of magnitude fits well the previous estimates given by Farinella *et al.* (1998) or Bottke *et al.* (2000). There are both "obvious" and "unexpected" features in this figure. Among the obvious results we notice that smaller objects (6489 Golevka) exhibit higher mobility than the large ones

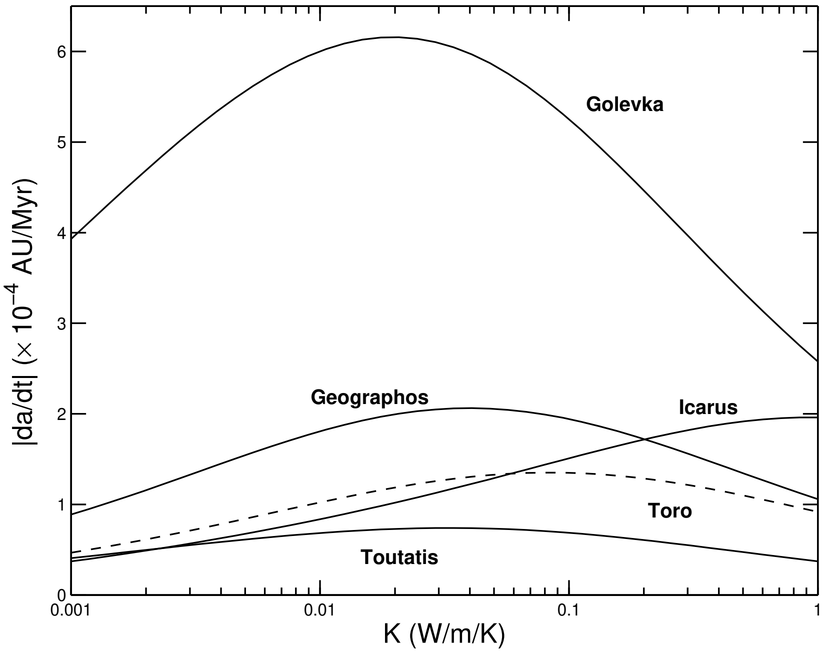

Fig. 1.— The estimated secular drift $|da/dt|$ of the semimajor axis due to the diurnal variant of the Yarkovsky effect for selected asteroids vs. the surface conductivity K. In the case of 1685 Toro the semimajor axis drift is positive (dashed line), while in all other cases the orbits decay (da/dt negative; solid lines). Nominal values of the spin axis orientation and radii (from Table 1) are assumed.

(4179 Toutatis). On the other hand, we also present results that have not been reported so far. In the case of Icarus, for instance, the higher diurnal mobility appears for higher surface conductivity which is just opposite to the previous experience (e.g., Farinella *et al.* 1998). This reversal is most probably caused by the very high eccentricity of the orbit. In some cases (4179 Toutatis and to a lesser extent also 1685 Toro and 1620 Geographos) the diurnal mobility of the semimajor axis depends only very weakly on the surface conductivity. This is, in fact, a favorable circumstance since this parameter is unconstrained by other observations as has been mentioned above.

The principal effects that may cause computed values of da/dt to be uncertain are: (i) badly estimated characteristic size of the body, (ii) non–sphericity of its shape and (iii) badly determined or non–stationary (precessing) spin axis. All these factors together may result in a factor of two or three of mismodeling the semimajor axis drift (see, e.g., Vokrouhlický 1998b). As far as the characteristic size of the body is concerned we have two comments. First, in cases where triaxial characteristics have been resolved (e.g., Toutatis and Geographos) from combination of the optical, infrared and radar observations, we have used an approximation by a sphere of the equivalent volume (see above). By doing so we at least keep approximately the same volume and thus mass of the body. However, in some cases the body might not be fitted well even with an ellipsoid, for instance Toutatis (Ostro *et al.* 1999b). Secondly, we recall that the semimajor axis drift (da/dt) scales inverse–proportionally with the characteristic radius of the body. As a result a change in the radius affects the semimajor axis mobility in a very simple way.

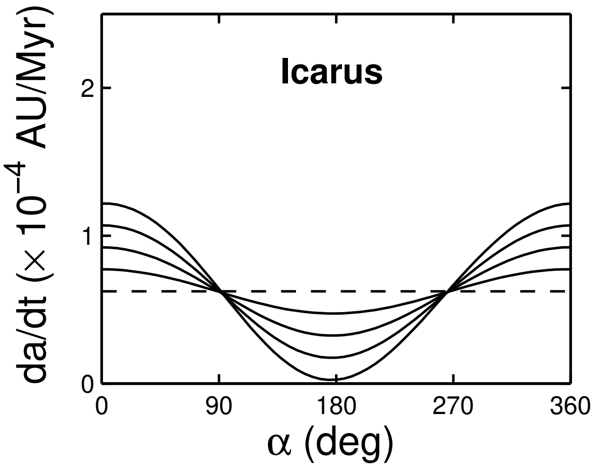

Fig. 2.— Sensitivity of the secular drift da/dt on changing the nominal orientation of the spin axis. The diurnal variant of the Yarkovsky effect assumed for 1566 Icarus (left) and 1620 Geographos (right). Low value of the surface thermal conductivity $K = 0.01$ W/m/K assumed. The curves of increasing amplitude of variation correspond to sweeping the spin axis of the asteroid along a cone with aperture 2.5, 5, 7.5 and 10 degrees, respectively, around the nominal orientation. The angle α (abscissa) parametrizes the position on the cone.

Next, we comment on the issue of the spin axis orientation. The pole characteristics (longitude and latitude) are usually determined up a few degrees of uncertainty (in the best cases). On the contrary, in several cases (4179 Toutatis or 1620 Geographos) we know the rotation state very precisely from the detailed analysis of the radar data. As expected, some bodies do not exhibit a simple (uniform) rotation about a spatially–fixed axis but rather tumble around the constant vector of the total angular momentum (as in the case of Toutatis; Ostro *et al.* 1999b). To understand the sensitivity of our results to changes in the orientation of the spin axis we have performed the following test. We have considered fictitious configurations with the spin axis sweeping a cone with some aperture around the nominal value of the axis orientation (given in the Table 1). We have taken 2.5, 5, 7.5 and 10 degrees, respectively, for the aperture angle. Fixing the value of the surface conductivity (to 0.01 W/m/K), we have computed the semimajor axis drift for bodies rotating about the fictitious spin axes (which position on the cone has been parametrized by an angle α). No changes in the rotation period were assumed. The results are shown in Figs. 2 and 3. In some cases (1620 Geographos and 4179 Toutatis), the results from the Fig. 1 are quite robust on changing the spin axis orientation since the da/dt–drift on even the 10 degree cone stay close to the central value. 1566 Icarus and 6489 Golevka show larger sensitivity on changes in the spin axis

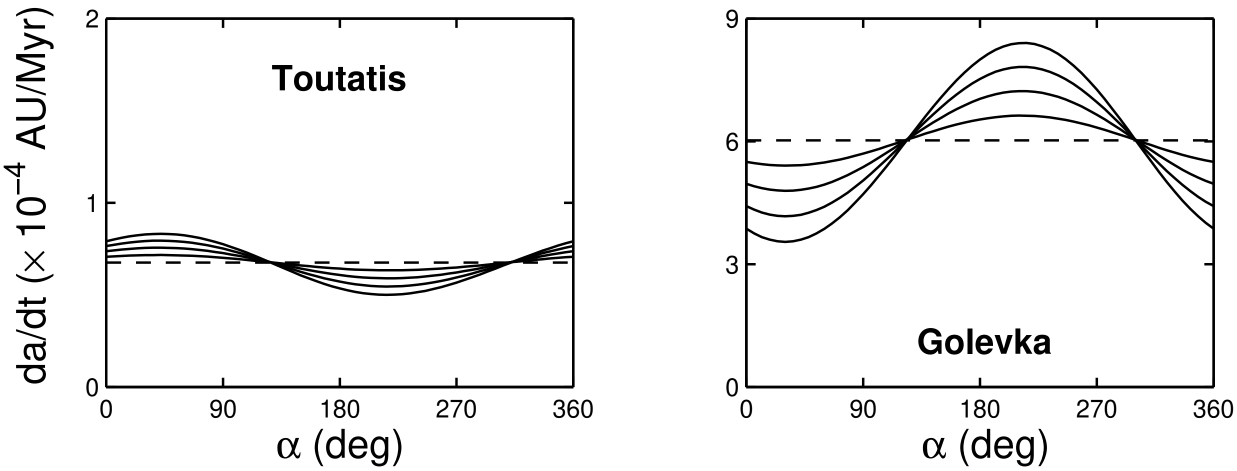

Fig. 3.— The same as in Fig. 2 but for 4179 Toutatis (left) and 6489 Golevka (right).

orientation. However, assuming that the spin axis is tumbling along the cone, we observe that the mean value of the semimajor axis drift remains close to the value derived from the configuration with the nominal orientation of the spin axis. Obviously, here we neglect the fact that tumbling period may be comparable to the rotation period, an effect that has been modeled precisely by Vokrouhlický (1998b). Any offset of the mean orientation of the spin axis with respect to the "nominal" value from the Table 1 may result in a net change of the semimajor axis drift. From the maxima and the minima of the oscillation cycles in Figs. 2 and 3 we have an indication of the amount of uncertainty introduced by possible spin axis errors.

3.2. Seasonal Yarkovsky effect

Figure 4 depicts the results of the mobility of the semimajor axis due to the seasonal effect. We have always used the higher precision model from Sec. 2.2.2, however we also checked reliability of the lower precision model (giving at maximum 10% different results). In general, the seasonal drift is always smaller than the diurnal drift, which is again in good agreement with the previous results of Farinella *et al.* (1998) or Bottke *et al.* (2000). Bodies with an insulating layer on their surface, $K \leq 0.1$ W/m/K, have typically negligible seasonal mobility, which is again an expected result. The same holds for larger mobility determined in the case of smaller bodies in our sample (6489 Golevka) and smallest mobility for the largest body (4179 Toutatis).

As in the case of the diurnal effect, the principal source of error of the previous results may emerge from the size considerations, non–sphericity and spin axis mismodeling. On top of these factors, Vokrouhlický and Brož (1999) discussed another aspect that may affect the computed seasonal value of da/dt. They showed that for bodies with a very thin low–conductive layer on

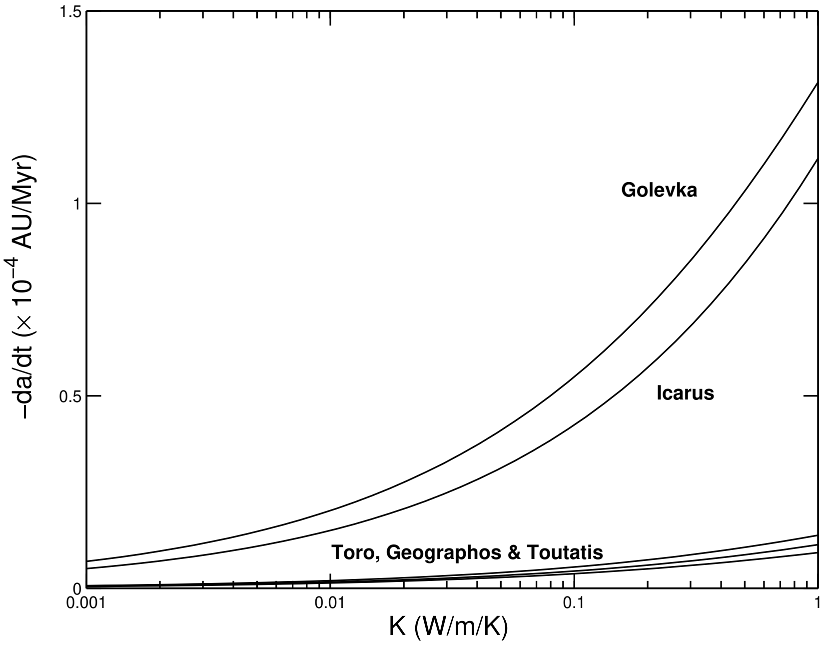

Fig. 4.— The estimated secular drift $-da/dt$ of the semimajor axis due to the seasonal variant of the Yarkovsky effect for selected asteroids vs. the surface conductivity K. In all cases the orbit decays. Nominal values of the spin axis orientation and radii from Table 1 are assumed.

the surface (regolith or porosity limited just to surface slab) the seasonal effect mobility may be enhanced by penetration of the seasonal thermal wave below this surface layer. The higher conductive core then helps increasing the thermal lag of the seasonal effect and thus the semimajor axis drift–rate. As a result the values of da/dt determined for $K \leq 0.01$ W/m/K might be increased by a factor of 5–10. However, even applying this factor the overall seasonal mobility is rather small in nearly all cases.

3.3. Total Yarkovsky effect and discussion

As was specified above, the total Yarkovsky perturbation represents a simple superposition of the diurnal and seasonal parts. Figure 5 shows such a composition of the results from Figs. 1 and 4. It is worth mentioning, that in the case of 6489 Golevka, 1620 Geographos and 1566 Icarus we have checked our results with those obtained by J. Spitale (personal communication; see Spitale and Greenberg 1999, 2000). Though his approach is fairly different from ours, the results match reasonably well. For 1620 Geographos we obtained nearly identical results. In the case of 6489 Golevka, our results indicate about half of the Yarkovsky mobility than obtained by Spitale, while in the case of 1566 Icarus our results are larger by a factor of about 1.5. In the next para-

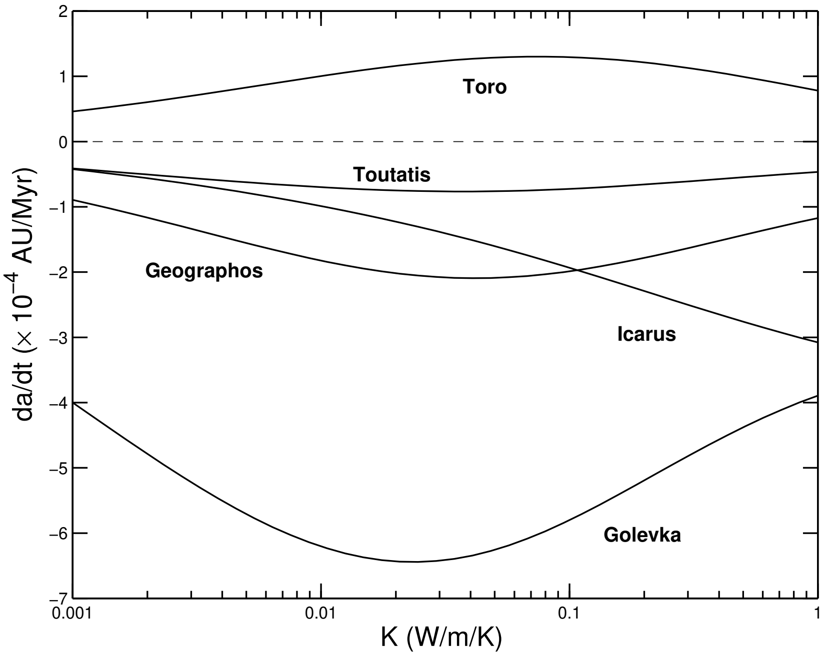

Fig. 5.— The estimated secular drift da/dt of the semimajor axis due to the superposition of both variants of the Yarkovsky effect for selected asteroids vs. the surface conductivity K. Nominal values of the spin axis orientation and radii from Table 1 are assumed.

graphs of this section we shall discuss some additional sensitivity tests and will also consider the object 1998 KY_{26}. We leave a detailed discussion of the potential detection of the Yarkovsky effect from the orbit determination of each of the asteroids to Sec. 4.

We can conclude that in the three cases out of five considered (1620 Geographos, 1685 Toro and 4179 Toutatis) the resulting Yarkovsky semimajor axis drift depends only very weakly on the surface conductivity value. This is in fact a very favorable circumstance, since it partially frees us from doubts about the uncertainty of our results stemming from the poorly known value of this parameter (we warn the reader, however, that this conclusion does not exactly apply to the more realistic situation when the surface conductivity changes along the orbit; see Sec. 2.1). The principal uncertainty of our results then concerns a possible mismodeling of the body's size and estimation of its albedo, and its non–spherical shape. The case of Golevka is illuminating because until the recently decisive results of Hudson *et al.* (2000) the size of this object was poorly known. The Hudson *et al.* result confirmed the estimate of Zaitsev *et al.* (1997), which was about twice as large as the estimate given by Mottola *et al.* (1997). This lower size estimate was associated with an unusually high albedo of 0.6, while the results of Hudson *et al.* and Zaitsev *et al.* include an albedo of 0.15.

With this case in mind, we may question the very high value of the 1566 Icarus albedo (0.4)

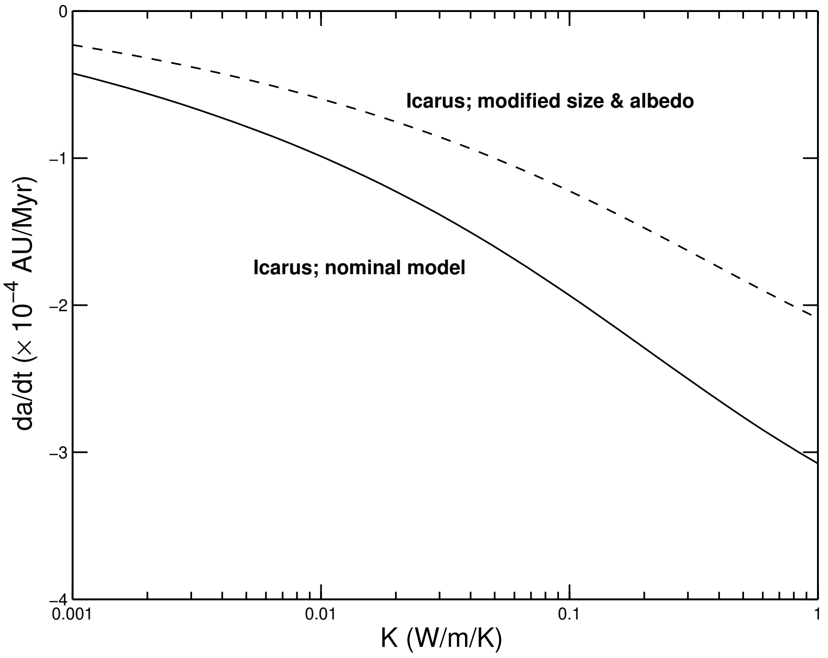

Fig. 6.— The estimated total secular drift da/dt of the semimajor axis of Icarus due to the Yarkovsky effect vs. the surface conductivity K. The solid line for the for the "nominal" Icarus' parameters (radius of 450 m and 0.4 albedo) from Table 1. Dashed line for a fictitious Icarus with $R = 900$ meters and lower albedo of 0.1.

and the corresponding possible underestimation of its radius ($R = 450$ m) reported by Veeder *et al.* (1989). We have thus decided to consider an alternative model for Icarus with twice the radius (900 meters) and a corresponding simultaneous decrease of the albedo to 0.1 (so that the absolute magnitude is unchanged). The total Yarkovsky drift–rate of the Icarus semimajor axis (i.e., diurnal plus seasonal effects) in both simulations is shown in Fig. 6. A decrease of the net semimajor axis drift by about 30–40% in the most important conductivity interval of 0.01–0.1 is apparent.

For completeness of our discussion, we note that the Icarus orbit determination history is somewhat interesting in the context of our work. Sitarski (1992) announced that his analysis of Icarus' optical data may reveal a non–gravitational effect perturbing its semimajor axis at the level of $(da/dt)_{\rm Sitarski} \simeq -(7.5 \pm 4.0) \times 10^{-4}$ AU/Myr (our units). This value is slightly larger than the expected Yarkovsky drift; only assuming a high value of the surface conductivity ($K \simeq 1$ W/m/K) allows our results to fall into the error–bar of Sitarski result. In the case of a lower value of the surface conductivity, which is more probable for Icarus, the semimajor axis drift determined by Sitarski is larger by a factor of about 5 than the expected Yarkovsky value. However, the large uncertainty of Sitarski's result suggests that his detection may be of only marginal quality. Indeed, Yeomans (1992) recomputed the Icarus orbit and found no need for secular change in its orbit (after he had corrected an error in his code that led him previously to a similar conclusion to Sitarski's;

Yeomans 1991). Our orbit determination with today's data also does not require any additional non–gravitational effect above the uncertainty of the observations.

A somewhat similar, but more complicated, history surrounds the orbit of 4179 Toutatis because of its two 1934 prediscovery observations. Sitarski (1998) argued that the nominal orbit of Toutatis, based only on modern observations from 1988, fails to match these early observations if only conservative forces are taken into account. By curiosity he observed that the mismatch might be cured by introducing an empirical acceleration $\mathbf{a}_{\rm pert} \simeq (\dot{a}/2a)\,\mathbf{v}$, where $\dot{a}$ is the solved–for mean change of the semimajor axis of the orbit. Sitarski (1998) observed that taking an empirical value of $(da/dt)_{\rm Sitarski} \simeq -58.4 \times 10^{-4}$ AU/Myr (in our units) may significantly improve the misfit of the 1934 observations. Though of the correct sign, Sitarski's value is nearly two orders of magnitude larger than the expected value due to the Yarkovsky effect (between 0.5–1 $\times\, 10^{-4}$ AU/Myr principally given by the diurnal variant of the Yarkovsky effect; see Figs. 1 and 5). Indeed, propagating back in time the mean anomaly effect given by the Eq. (30), and taking into account $da/dt \simeq -0.5 \times 10^{-4}$ AU/Myr, we would expect a right ascension displacement of about 0.2 arc–second, far too small to explain the misfit of the 1934 observations.

The above contradiction can be eliminated with one of the following explanations: (i) the 1934 observations are either mistaken or, at least, subjected to larger uncertainty than assumed by Sitarski, (ii) our solution for the theoretical drift of the Toutatis semimajor axis due to the Yarkovsky effect is seriously underestimated or (iii) there is an additional non–gravitational effect acting on the Toutatis' orbit that is exceeding the Yarkovsky effect by two–orders of magnitude. Any of these possibilities (or a combination of them) may be correct, but presently we are not able to discriminate between them. In our opinion, however, the items (ii) and (iii) are less likely than the hypothesis in (i). Indeed, a statistical analysis of the observational errors for that epoch and the observatory involved indicates an expected RMS error of 2.7 arc–seconds for these early data (M. Carpino, personal communication; see `http://newton.dm.unipi.it/neodys/` where these data are published for each observatory). The prediscovery observations then fall within 3σ and there is no strong reason to conclude that they indicate a phenomenon to be explained.

Finally, we pay attention to the Yarkovsky perturbation of the small asteroid 1998 KY_{26}. Although this body has been observed by radar only once (June 1998) it represents a new type of object that may be very valuable in detecting the Yarkovsky effect and testing current methods. Since there is a possibility that during the next years we may monitor the orbit until its next close approach to the Earth in June 2024 (see Sec. 4.5) and also it is likely that in the future we shall accumulate data about similar bodies in the Earth's vicinity, we have included discussion of 1998 KY_{26} in this paper. The principal factor that favors measuring the Yarkovsky effect is the small size of 1998 KY_{26}: $R \simeq 15$ meters (Ostro *et al.* 1999b). Figure 7 shows the expected drift of the asteroid semimajor axis due to the diurnal and seasonal variants of the Yarkovsky effect. Unfortunately the 1998 observations of this object did not reveal a precise orientation of the spin axis, though it seems likely to be roughly perpendicular to the ecliptic plane (P. Pravec; personal communication). Since the inclination of the orbit is low ($\simeq 1.5$ degree) this situation would favor

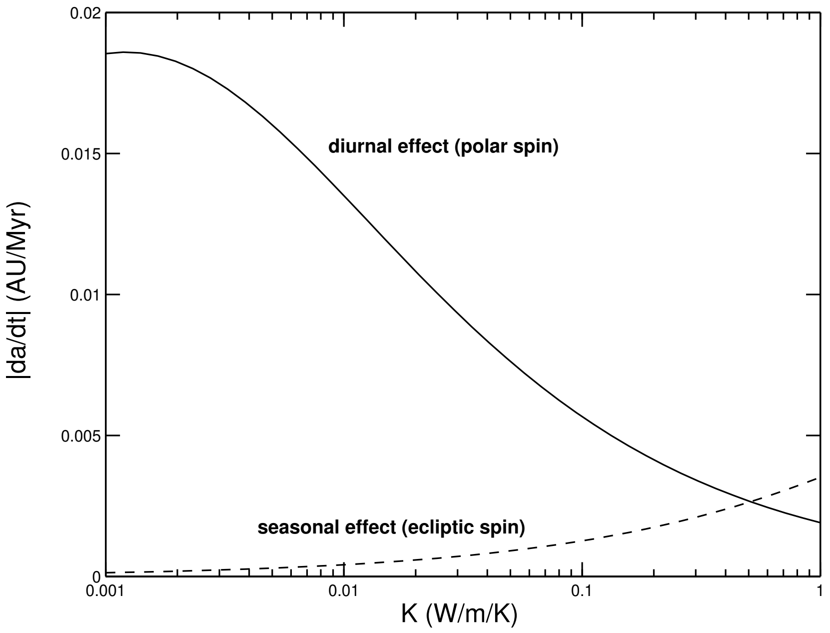

Fig. 7.— The estimated secular drift $|da/dt|$ of the semimajor axis of the small object 1998 KY_{26} vs. the surface conductivity K. The solid line for the diurnal variant of the Yarkovsky effect and the spin axis perpendicular to the ecliptic plane (a more likely situation; P. Pravec, personal communication), the dashed line for the seasonal variant of the Yarkovsky effect and the spin axis along the orbital node (in ecliptic; for this latter case the diurnal effect vanishes and the seasonal effect is maximized).

the diurnal variant of the Yarkovsky effect and inhibit the seasonal variant (solid line in Fig. 7). For the sake of comparison we have also simulated the case when spin axis would be in the plane of the ecliptic (along the nodal line). The contribution of the diurnal effect would be minimum, while the seasonal effect would be maximized (dashed line in Fig. 7).

Assuming the ecliptic–pole orientation of the spin axis, we note a diurnal Yarkovsky mobility of the 1998 KY_{26} semimajor axis several orders of magnitude larger than the other objects we have discussed so far. At the time of its next close approach to the Earth (June 2024) the predicted orbit displacement ranges in the interval of 1600 km (for high conductivity $K \simeq 1$ W/m/K) up to about 4500 km (for very low conductivity $K \simeq 0.01$ W/m/K). However impressive might be such number, and it indeed provides a large potential for probing the Yarkovsky effect, we must also warn the reader that it might be of about the same order as the orbit uncertainties if the orbit is not carefully monitored (notice that 1998 KY_{26} has been observed for only about two weeks in summer 1998). In Sec. 4.5 we envisage an optimum observation program for this object so that at its next close approach (June 2024) it might be well–suited for the Yarkovsky effect study.

4. Simulation of future apparitions

After gaining insight concerning the order of magnitude of the possible perturbation due to the Yarkovsky effect, its dependence on the unconstrained model parameters (such as the surface conductivity) and some other issues, we now face the question of the observability of the Yarkovsky effect. Obviously, this task demands not only to know the expected orbital perturbation, but more importantly, we must compare the predicted perturbation with the orbit determination uncertainty. Only when the uncertainty with which we know the given orbit, and with which we may expect to observe the orbit in the future, is smaller than the Yarkovsky perturbation may we assume the effect is detectable.

First, we note that we have performed orbit determination for all bodies in Table 1. The observational datasets comprised all optical and radar observations available to us as of November 1999. The optical observations were obtained by subscription from the Minor Planet Center, and the radar observations are publicly available from the Jet Propulsion Laboratory at `http://ssd.jpl.nasa.gov/radar_data.html`. The combined datasets are republished at `http://newton.dm.unipi.it/neodys/`.

The force model included planetary perturbations to the post–Newtonian order $1/c^2$ (c is the velocity of light) with planets modeled as massive monopoles (the so called EIH approximation). Optionally, we incorporated also the solar quadrupole J_2 term as adopted by the JPL DE405 ephemerides. Three massive asteroids (Ceres, Pallas and Vesta) were also included in our model. As far as the radar data are concerned, we used the procedure outlined in Yeomans *et al.* (1992). Relativistic and ionospheric delay effects of the radar signal were applied. We also included careful treatment of the time scales, adopting the TDB time scale as a fundamental independent variable in our model. When necessary, in particular for the Earth rotation model, a transformation to the TDT time scale was performed. Our force model included both variants of the Yarkovsky acceleration.

In each of the cases we performed two orbit determinations, one with the nominal model that does not contain the Yarkovsky acceleration and one with a model including the Yarkovsky acceleration. In none of the cases have we observed a statistically important change of results. From this we conclude, that the Yarkovsky effect cannot be detected using the currently available data since the corresponding perturbation is well within the orbital uncertainty. A closer look at the formulas (29) and (30) helps understand this conclusion. First, we do not have a very long series of precise optical observations for NEAs, which would aid in the observability of the mean anomaly effect (30). The radar measurements are thus necessary for a tight constraint of the orbit. The radar measured orbits are of two types: (i) either we have available two radar apparitions that are favorably well separated in time ($\Delta_{10}t$ is large; e.g., 1566 Icarus and 1685 Toro) but they are of rather low quality, or (ii) we have available two high–quality radar measurements that are not separated enough in time ($\Delta_{10}t$ small; e.g., 1620 Geographos, 4179 Toutatis or 6489 Golevka). Obviously, when only one radar measurement is available (e.g., 1998 KY_{26}) the orbit is not constrained enough.

Note that the time separation $\Delta_{10}t$ of the first and last radar measurement is a decisive factor since the Yarkovsky perturbation propagates quadratically with time. This remark also provides a strategy for determination of the Yarkovsky effect in the future. By considering the next close approach to the Earth we shall focus on cases with the orbit constrained well enough to possibly reveal existence of the Yarkovsky perturbation.

Before we embark on discussing individually the cases of asteroids from the Table 1, we mention that we have discarded 1685 Toro from further considerations. This does not mean that the object might not be potentially interesting in the context of our work, but the present orbit uncertainty does not allow the detection of the Yarkovsky effect at the next apparition (and probably even in the next two apparitions). The low quality of the previous radar measurements (in 1980 and 1988) is the principal reason for this conclusion. However, since Toro will appear at the close approach regularly in the next decades (close approaches in Jan 2008, 2016, 2024 and 2032) the orbit might contain valuable information about the Yarkovsky effect if regularly observed by radar and a precise model of the asteroid is determined. However, we postpone a detailed discussion of this case for future work.

4.1. 6489 Golevka

Golevka is a very interesting target for attempting the detection of the Yarkovsky effect. It has been observed by radar in 1991 and 1995. Both delay and Doppler measurements were obtained on the two occasions. The 1995 measurement analysis allowed reconstruction of Golevka's shape model and to reduce the radar astrometric data to the center–of–mass of the asteroid. The formal uncertainty of these measurements are about 30 meters in range. Complementary to these precise measurements, the appreciable semimajor axis mobility of Golevka's orbit due to the Yarkovsky effect (Fig. 5) strongly favors its detection. The only unlucky circumstance is a lack of radar astrometric measurement during the 1999 close approach of this object, although such data may yet be forthcoming (S. Ostro; private communication). The next possibility to take radar observations for this asteroid occurs in June 2003. Our effort in the rest of this section is to demonstrate that radar measurements at this epoch could indicate the Yarkovsky perturbation on this orbit.

Assuming a surface thermal conductivity of 0.01 W/m/K we obtain the approximate value $da/dt \simeq -6 \times 10^{-4}$ AU/Myr for the semimajor axis drift. Equation (29) then yields an estimate of 15.2 km for the orbit displacement during the time interval bracketed by the first (1991) and the last (2003) radar observations. If the surface conductivity is an order of magnitude larger (0.1 W/m/K) this estimation does not change markedly. In either case these perturbations are appreciably larger than the formal error of the radar measurements (that already include the shape model uncertainty). We thus need to focus on understanding the orbit determination error at the epoch of June 2003. The methodology of our work, similar for all cases below, will be described in some detail in the next few paragraphs.

First, we perform the orbit determination by taking into account all available observations and the nominal force and measurement model that does not include the Yarkovsky effect. At the weighted midpoint of these observations we construct the initial state vector together with a complete covariance matrix analysis. Then, we propagate these initial data to the epoch of next close approach of the object, for instance June 2003 in the Golevka's case, and project the uncertainty hyper–ellipsoid onto the range (R) and range–rate (dR/dt) plane. These are basically the radar observables. The algorithm to perform this projection is essentially the same used to project on the celestial sphere (with coordinates right ascension and declination), and is described by Milani (1999) in two versions, linear and semilinear. (Because of the very accurate orbit determination needed to detect the Yarkovsky effects, the linear approximation is satisfactory in all cases of interest for this paper.) In this way the radar observation at a given time can be predicted to belong to a confidence region which is the inside of an ellipse in the $(R, dR/dt)$ plane. For sake of a more detailed analysis, we compute the confidence region not only at the instant of the close approach of the nominal orbit but also a few days before and after that instant. The `OrbFit` software package has been updated, starting from version 2.0, to allow for both processing and predicting radar observations with the necessary accuracy.

Second, we perform the same orbit analysis with a force model that includes the Yarkovsky effect. As mentioned above, the orbit determination with presently available observations yields the same residual size in both cases. Typically, both procedures lead to a fit of the radar data and the optical astrometry below a weighted 1–σ uncertainty of the observations. The difference between the fits with the standard model and the fits with the Yarkovsky–included model is at the level of the statistical noise in the observations. However, having computed the second solution we may propagate, *with* the Yarkovsky acceleration, the initial data (i.e. the initial state vector and the covariance matrix) to the epoch of the next close approach when we shall have a possibility to take radar measurements. We again project the uncertainty hyper–ellipsoid onto the range vs. range–rate plane. The comparison of the uncertainty regions of the two solutions may indicate whether these future data will have a capability to reveal the Yarkovsky effect or not. In particular, if the 3–σ ellipsoids of the two solutions in the R–dR/dt plane do not overlap we have a good statistical confidence that the Yarkovsky effect might be detected at this level (3–σ is just a conventional measure that corresponds to the 98% probability if the errors have gaussian statistics).

Let us now consider this method for Golevka and its next apparition in June 2003. Figure 8 shows the range vs. range–rate plane projections of the 3–σ uncertainty ellipsoids of the nominal solution (dashed ovals) and the Yarkovsky–included solutions (solid ovals). The solution for the epoch of the closest approach of the nominal orbit is labeled 0 and we also plot solutions for ± 3 and ± 6 days around the close approach. The center of the nominal–orbit uncertainty ellipsoids at each of the epochs were shifted to the origin of the R–dR/dt plane. The centers of the Yarkovsky–included uncertainty ellipsoids were shifted accordingly and are shown by the solid boundaries in Fig. 8. In this solution we assumed a surface thermal conductivity of Golevka of 0.01 W/m/K and the other physical parameters as in Table 1.

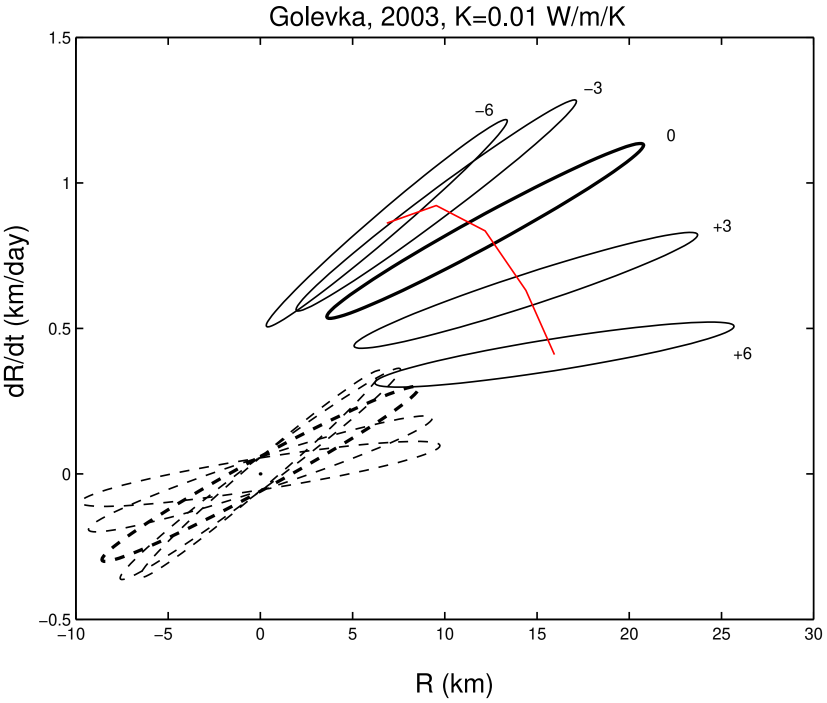

Fig. 8.— Projection of the orbit solution uncertainty ellipsoid onto the range R and range–rate dR/dt plane for next close approach of 6489 Golevka in May 2003. The formal 3–σ ellipsoids considered for both nominal orbital solution without the Yarkovsky effect included (dashed lines) and the solution extended by the Yarkovsky effect (solid lines). Different ellipsoids correspond to five observation dates, labeled with numbers indicating the number of days after the closest approach of the nominal orbit. The origin $(0,0)$ refers to the center of the nominal orbit ellipsoid at each day. For the Yarkovsky effect we assumed 0.01 W/m/K for the surface thermal conductivity.

We note that the range displacement of the two solutions at the closest approach is about 12 km, in a fairly good agreement with the previous simple estimation. As expected, the range uncertainty is much larger than the 2003 measurement error, but the fact that the 3–σ ellipsoids do not intersect in the R–dR/dt plane is the salient point. Even more important is that this conclusion holds also for epochs both before and after the close approach. From Fig. 8 we would conclude that the Yarkovsky effect could be detected by radar observations of Golevka in 2003. Furthermore, this conclusion can be extended to a fairly wide range of surface thermal conductivities since, according to Fig. 5, the Yarkovsky mobility for Golevka is weakly sensitive to variations in thermal conductivity, especially in the most likely range of 0.001–0.01 W/m/K.

We mention finally that for Golevka the next close approach after 2003 does not occur until June 2046, thus the 2003 radar observations should be given very high priority.

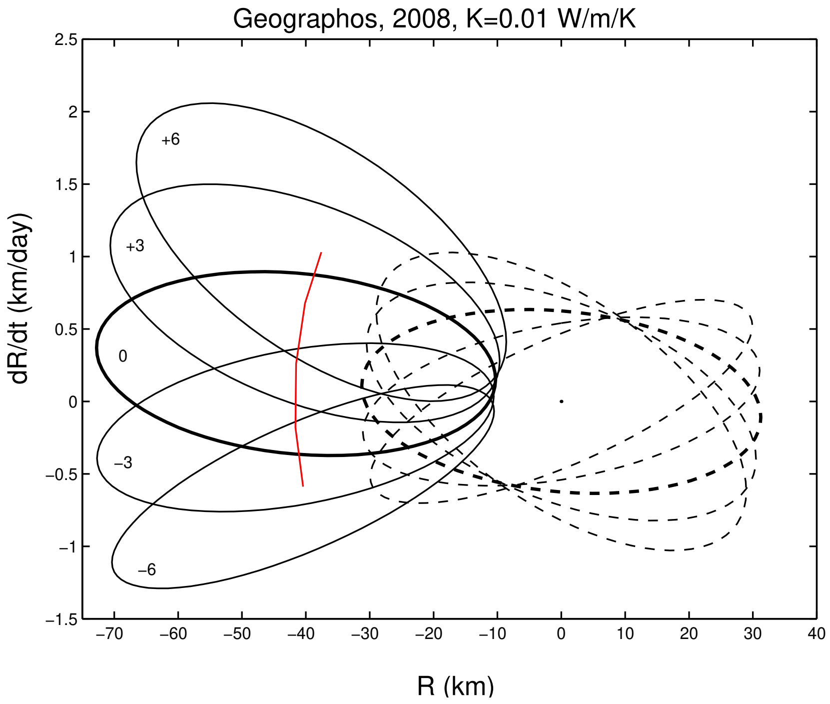

Fig. 9.— Projection of the 3–σ uncertainty ellipsoids onto the range (R) vs. range–rate (dR/dt) plane for the next close approach of 1620 Geographos in March 2008. Notation as in Fig. 8. In particular, the Yarkovsky–included solution shown by solid lines (the surface thermal conductivity $K = 0.01$ W/m/K) and the solution not including the Yarkovsky effect shown by dashed lines.

4.2. 1620 Geographos

Like Golevka, Geographos is another very good target for investigating the Yarkovsky perturbation. Two radar apparitions are available out of which only the second, in August 1994, is of high quality (Ostro *et al.* 1996). The former, taken in February 1983, are of lesser quality but still represent a valuable constraint on the orbit. Moreover, in the case of Geographos the optical astrometry data span back to 1951, thus they give another important constraint.

According to results in Fig. 5 the Geographos orbit undergoes a rather fast inward semimajor axis drift that is to a large extent independent of the exact value of the surface thermal conductivity. We shall thus use 0.01 W/m/K for this parameter throughout this section. Estimating the formal displacement by using Eq. (29) during the 1983–1994 period we get $\Delta\rho \simeq 10$ km. However promising, there are several reasons why such a displacement is not enough to reveal existence of the Yarkovsky effect. Most importantly, the 1983 radar observation has a formal error of about 4.5 km. Secondly, Geographos has a rather complicated shape with the axes of about 5.11/2.76/1.85 km (Ostro *et al.* 1995, 1996), a fact that adds to the uncertainty of the 1983 observation (since that was not reduced to the center–of–mass of the asteroid). Besides these two observational reasons, we note that Geographos' elongated shape, together with possibly complicated spin axis evolution, might partly invalidate our estimate of the Yarkovsky semimajor–axis drift by a factor of about 2–3. Our work will thus again focus on understanding whether observations at the next close approach of Geographos, in March 2008, may reveal the Yarkovsky perturbation.

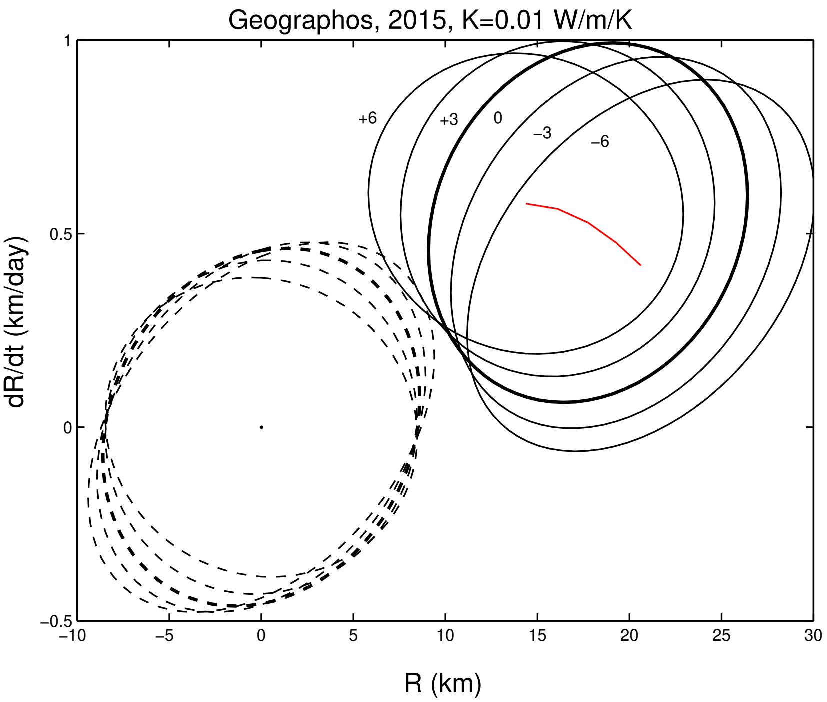

Fig. 10.— 3–σ uncertainty ellipsoids in the range vs. range-rate plane for Geographos close approach in March 2015. Aside from the currently available observations, the solution also assumes a one week astrometric campaign and three radar observations during the 2008 close approach (see the text for more details). The notation is as in the previous figures.

Figure 9 shows the projections of the 3–σ uncertainty ellipsoids of the nominal and Yarkovsky–included solutions in March 2008 (we again trace the orbit in the interval ± 6 days around the close approach of the nominal orbit). The mean range displacement of the Yarkovsky–included orbit is about 41.5 km, which corresponds fairly well to the estimate of 47 km obtained from the simple formula (29). We note that the uncertainty ellipsoids of the two solutions partly overlap so that determination of the Yarkovsky effect still might not be decisive, though there is a substantial chance that the effect will be apparent. In this respect however, we admit that our thermal model for Geographos might be oversimplified (see our comments above). Developing a detailed, Geographos–tailored thermal model in the future would be of great importance but it is beyond the scope of this paper.

However, even assuming the "worst case situation", i.e. the 2008 radar observations at the

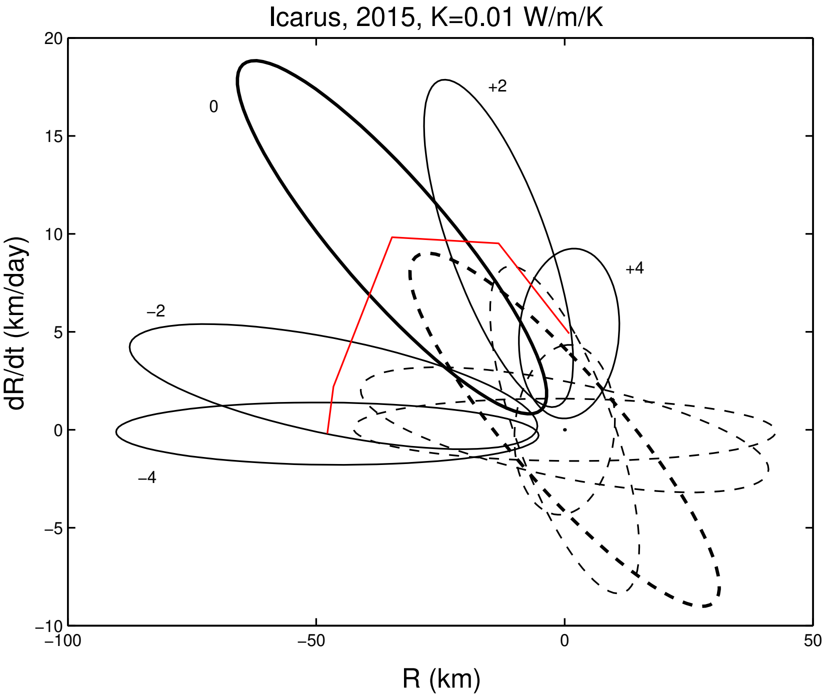

Fig. 11.— Projection of the 3–σ–uncertainty ellipsoids onto the range (R) vs. range–rate (dR/dt) plane for the next close approach of 1566 Icarus in 2015. The Yarkovsky–included solution is shown by the solid lines ($K = 0.01$ W/m/K surface conductivity), while the solution without the Yarkovsky effect is shown by the dashed lines.

overlap of the uncertainty ellipsoids shown in Fig. 9, we may perform the following test. We have simulated three delay observations by radar in mid March 2008 that fall in the mentioned overlap of the two uncertainty areas and assumed their formal error of 100 meters. Then we considered this new set of the observations and performed the orbit determination analysis with the two models (nominal and Yarkovsky–including). We have propagated the obtained initial state data until the next close approach of Geographos in March 2015. The 3–σ uncertainty ellipsoids projected into the R–dR/dt plane are shown in Fig. 10. We notice that the uncertainty areas are disconnected at the 3–σ level, a feature that is to be expected due to the secular character of the Yarkovsky perturbation. Notice that the 2015 displacement of the two solutions in Fig. 10 is only about 17.8 km, hence the disconnection is essentially the effect of reduced orbit uncertainty. This is understandable since we assumed a good quality radar observation in 2008 that has been added to the data, but the reduced separation deserves a brief comment. It might appear puzzling why this displacement is smaller than in 2008. There are two reasons: (i) the weighted center of the observations had shifted towards later epoch (since the 2008 radar observation contribute) so there is a shorter time interval over which the Yarkovsky perturbation accumulates, and (ii) we used a "worst case scenario" for the 2008 observations by placing them in the overlap of the uncertainty ellipsoids of the two solutions. This means, that in fact they do not fit well either of the two solutions and "forces" them to get closer each other. As a result of these two factors the 2015 Yarkovsky–displacement in this scenario becomes only 17.8 km as shown in Fig. 10. Had the observation suited better one of the solutions the divergence at 2015 will be larger.

We may thus conclude that the 2015 apparition data of Geographos will very likely allow us to test for the presence of the Yarkovsky effect on its orbit. However, a Geographos–tailored thermal model, including in particular its very elongated shape, would be necessary to exploit in detail this information.

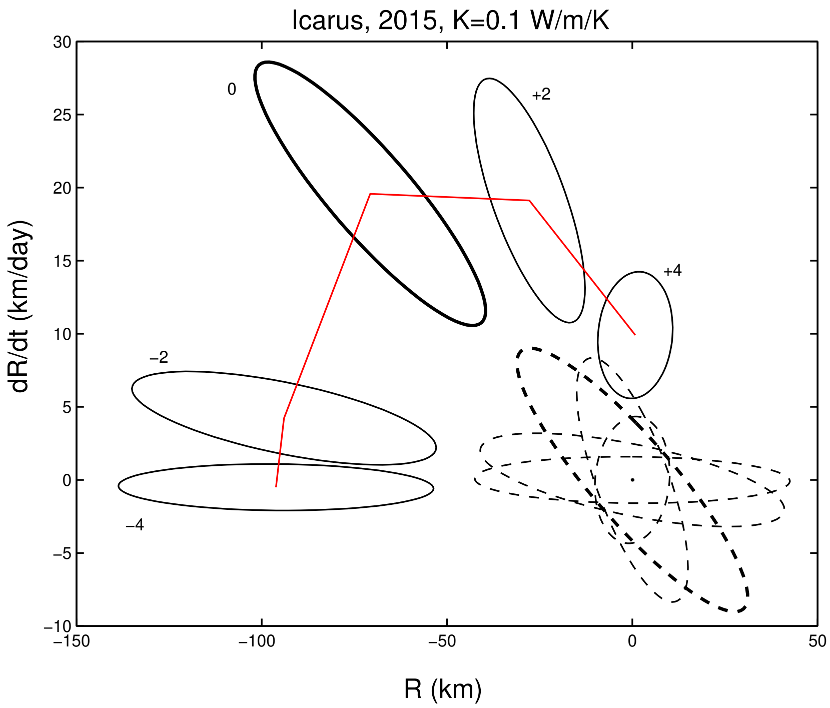

Fig. 12.— The same as in Fig. 11 but for the Yarkovsky solutions with the surface conductivity of 0.1 W/m/K.

4.3. 1566 Icarus

Icarus, with its very elongated orbit and close encounters to all terrestrial planets, presents a challenge both for the orbital dynamics and for computation of the Yarkovsky effect. Its low perihelion has also made it a target of studies attempting to test relativity theory (e.g., Lieske and Null 1969; Shapiro *et al.* 1971). Although Icarus was the first radar–detected asteroid in 1968 (Goldstein 1969), and was later observed during its 1996 apparition, the radar data are unfortunately of lower quality since only Doppler observations were obtained. Moreover, though quite numerous and dating back to 1949, the sparse and often erroneous optical astrometry measurements make the uncertainty of the orbit determination quite large so that the present orbit solution cannot reveal the existence of the Yarkovsky effect.

The next possibility for radar observations of Icarus will occur in June 2015. Assuming the time base from the first radar observations, the formal estimation of the orbit displacement due to the Yarkovsky effect is about 110 km for $da/dt \simeq -0.8 \times 10^{-4}$ (i.e. $K \simeq 0.01$ W/m/K) and even 248 km for $da/dt \simeq -1.8 \times 10^{-4}$ (i.e. $K \simeq 0.1$ W/m/K). The results of the uncertainty analysis outlined above are shown in Figs. 11 and 12. Because of the geometry of the Icarus' orbit, the above estimated range displacement is reduced by about a half, which is still an appreciably large value. However, the orbit uncertainty expressed by the size of the 3–σ uncertainty ellipsoids is also quite large, reflecting the poorer quality observations than in the previous cases of Golevka or Geographos. When the lower surface thermal conductivity is assumed (Fig. 11) the nominal orbit and Yarkovsky–included orbit uncertainty ellipsoids overlap to some extent, while the case with higher thermal conductivity (Fig. 12) is more favorable for detecting the Yarkovsky effect.

From August 2000 until the close apparition in 2015 Icarus could be observed optically during several periods when its visual magnitude decreases below $\simeq$ 17th magnitude (so that these observations would not require a very powerful telescope). Such optical observations would better constrain the 2015 uncertainty ellipsoid in the radar–observables plane and thus allow a greater possibility of detecting the Yarkovsky effect on Icarus' orbit.

4.4. 4179 Toutatis

Very high quality radar measurements at two Toutatis apparitions, in 1992 and 1996, are presently available. Both sets are referred to the center–of–mass of Toutatis and have a range uncertainty at the level of 75 meters (the 1996 data are even twice as good). This presents Toutatis as a potentially good target for investigation of the Yarkovsky effect despite a somewhat smaller Yarkovsky drift of its semimajor axis, principally due to its large size (see Fig. 5). On the other hand, a weak dependence of the resulting Yarkovsky perturbation on the surface conductivity reduces the uncertainty of our Yarkovsky model for this body. However, although they are very good, the 1992 and 1996 radar observations do not define a long enough temporal baseline for detection of the Yarkovsky perturbation. On the other hand, we are facing a sequence of Toutatis close approaches in 2000, 2004, 2008, and 2012. Hereafter, we investigate whether regular radar observation of Toutatis at each of these occasions might ultimately reveal the Yarkovsky perturbation on its orbit. We always assume nominal parameters of the Yarkovsky model from Table 1 and surface conductivity equal to 0.01 W/m/K, which we believe to be a probable mean value for this asteroid.

Using the current optical and radar observations of Toutatis, we have repeated the above analysis for the October 31, 2000 close approach. The 3–σ uncertainty regions of the two solutions projected onto the R–dR/dt plane are shown in Fig. 13. They overlap to a large extent, meaning

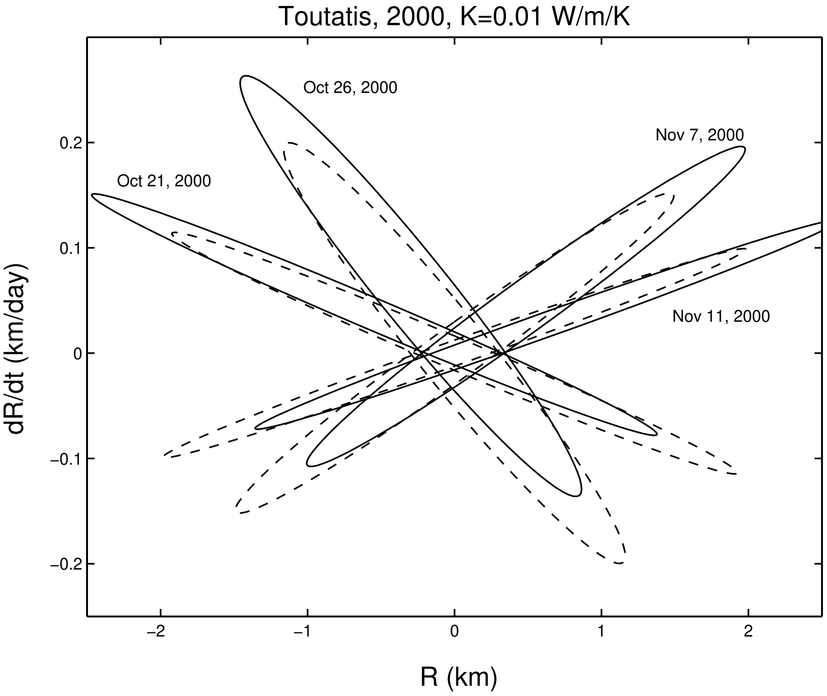

Fig. 13.— The 3–σ uncertainty ellipsoids projected onto the range (R) vs. range–rate (dR/dt) plane for the October/November 2000 (the close approach of Toutatis appears on Oct 31). Notation as in the previous figures. The Yarkovsky solution corresponds to the surface conductivity of 0.01 W/m/K.

that the potential radar observations in 2000 would not be conclusive about the existence of the Yarkovsky perturbation on Toutatis' orbit.

To more fully consider Toutatis' orbit we shall assume in the next paragraphs that precise radar observations have been taken during each of the successive close approaches to the Earth. Each time the uncertainty ellipses in the range vs. range–rate plane at the following close approach are reanalyzed, and the possibility to detect the Yarkovsky effect is considered.

As an example we show in Fig. 14 the comparison of the nominal model and the Yarkovsky–included model uncertainty projections onto the R–dR/dt plane in September 2004. Two delay observations during the previous close approach (in October 2000) were simulated with formal uncertainty of 40 meters and added to the dataset of the current observations. We notice that the uncertainty regions of the two solution are partially separated but not completely disconnected at the 3–σ level. Moreover, the principal shift occurs at the range–rate direction by a value that is comparable with the radar technology performance. For instance, the best Doppler accuracy for the the 1996 Toutatis observations in range–rate are about 0.1 km/day.

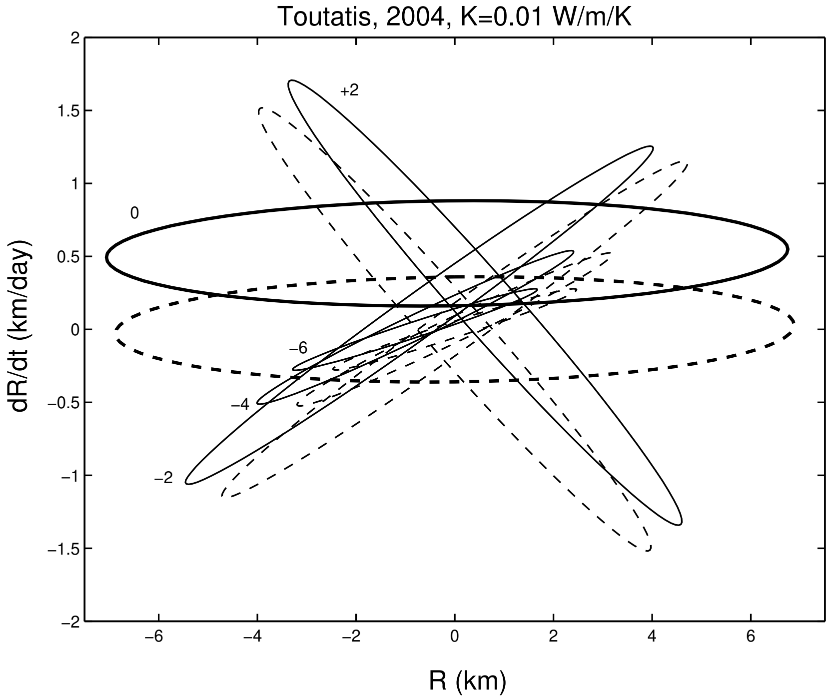

Fig. 14.— The same as in Fig. 13 but for the September 2004 close approach of Toutatis. The solution is based on the present Toutatis observations plus two simulated radar delay measurements during the October 2000 close approach to the Earth.

Continuing the analysis, we have simulated four delay measurements during the September 2004 Toutatis apparition in the overlapping zone of the uncertainty ellipsoids of the two models shown in Fig. 14. Then, we propagate the newly determined orbit to the following close approach in November 2008. The results in the R–dR/dt plane are then shown in Fig. 15. The uncertainty regions become highly stretched, having the principal axis aligned with the apparent motion direction. The phenomenon is a consequence of the previous (2004) close approach to the Earth, notably its unusually small minimum distance to the Earth (only about 0.01 AU compared to about 0.05 AU for the other close approaches). A closer look at the results indicate that the 3–σ uncertainty regions of the two models actually are disconnected, though they nearly touch. However, the distance between the two confidence regions is too small with respect to the current accuracy in range–rate. Thus confirmation of the Yarkovsky effect on Toutatis is possible, but not certain, with the 2008 data. However, the observations during the last close approach in the series, in December 2012, should reveal the Yarkovsky effect. In this case we have verified that observations from the model without the Yarkovsky effect cannot be fit well with the model including the Yarkovsky effect (and vice versa). Notice, that adding radar observations in 2012 means already a fifth consecutive apparition precisely measured by the radar technique.

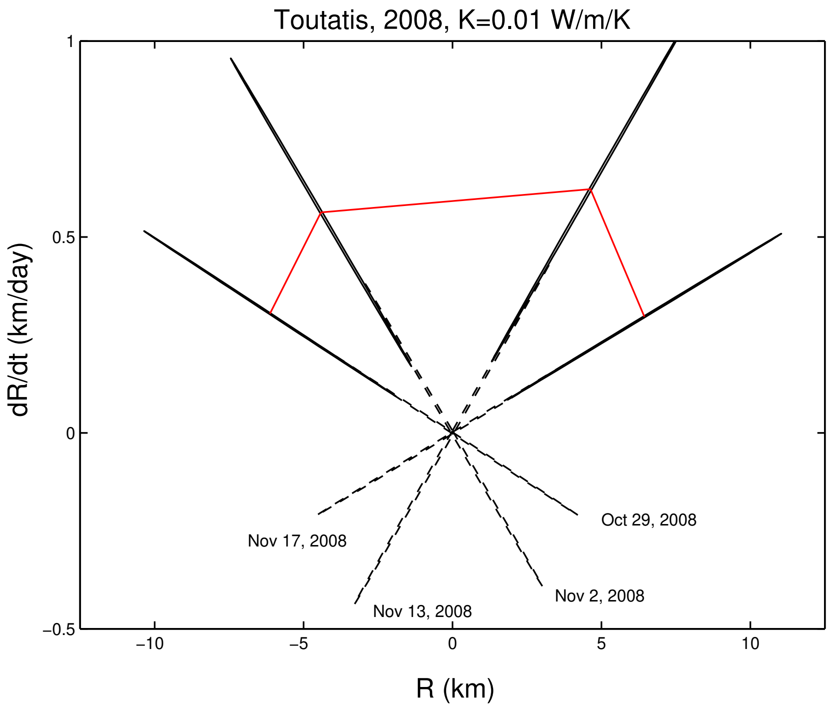

Fig. 15.— The same as in Fig. 14 but for the November 2008 close approach of Toutatis (close approach appears on Nov 9). The solution is based on the present Toutatis' observations supplemented by six simulated delay measurements during the October 2000 and September 2004 close approaches to the Earth.

Trying to summarize the above analysis we may conclude that, although the 2000–2012 radar observations of Toutatis are perhaps unnecessary from the point of view of shape modeling, they would be of great significance for the orbit determination of this asteroid. This conclusion is supported not only by our analysis of the possible Yarkovsky perturbation, but also by the still not conclusively solved problem of the 1934 prediscovery observations. We do not rule out the possibility that the correct force model for Toutatis still hides some unnoticed surprise, though we prefer the more "conventional" conclusion of assuming measurement errors in the 1934 observations (see our discussion in Sec. 3.3).

Finally, we note that the Yarkovsky effect is anyway not expected to be large enough to invalidate the conclusions of Ostro *et al.* (1999a) about the subsequent close approaches of Toutatis, because the uncertainty in position due to chaoticity of its orbit propagates exponentially (and thus faster than due to the Yarkovsky effect).

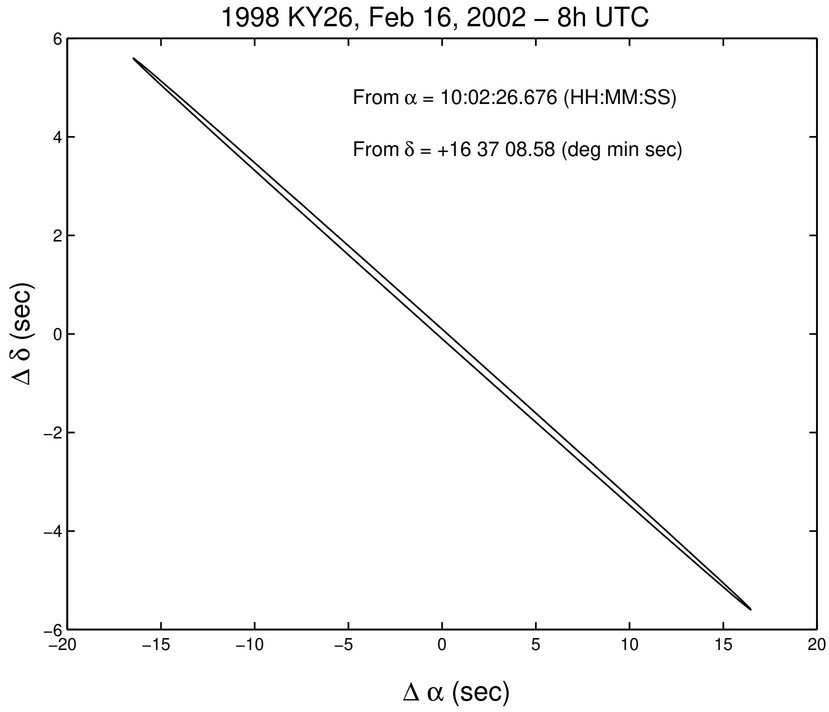

Fig. 16.— Orbit uncertainty (3–σ) ellipsoid projected onto the sky plane (right ascension and declination) for 1998 KY_{26} computed in Feb 16, 2002 (8h UTC). Coordinates are relative to the nominal position noted in the figure. At this epoch the object visual magnitude will be 24.7 at solar elongation of 176 degrees (see Table 2).

4.5. 1998 KY_{26}

We have already mentioned in Sec. 3.3 that the asteroid 1998 KY_{26} is a prototype of a new class of objects that might be ideally suited for studying the Yarkovsky effect. We thus devote the last part of this paper to outline an ideal schedule of fully exploiting 1998 KY_{26} to study the Yarkovsky effect. Such care is necessary since we presently have available only less than two weeks of observations from the summer of 1998. Objects of this size are frequently lost, which luckily should not be the case of 1998 KY_{26} thanks to the radar observations taken shortly after discovery.

The nearest possibility to observe this object in the future occurs on Feb 16, 2002, when it will have a visual magnitude of 24.7 at nearly zero phase. Though still very faint, this object should be observable by the better modern telescopes. Moreover, the recovery uncertainty at this epoch, shown in Fig. 16, is quite moderate so that no extraordinary effort would be needed to perform this observation. We have listed the majority of the other observational possibilities until the next close approach in Table 2 (considering only epochs when the apparent magnitude is smaller than 25). Though challenging, all observations at all epochs listed in the Table 2 are possible even with

Table 2: Observation opportunities for 1998 KY_{26} before the next close approach at May 2024 (in all cases the sky–position uncertainty is less than one arc-minute). Of particular interest is the second apparition in 2013, since the geocentric distance of the object would be only 0.12 AU. A possible radar ranging at this epoch, not considered in the "schedule" outlined in the text, would be valuable.

Date	visual magnitude	elongation (deg)
2002, Feb 16	24.7	176
2006, Jan 9	25.0	178
2009, Dec 2	24.3	179
2013, Mar 17	23.9	174
2013, Sep 20	23.4	115
2017, Jan 29	25.0	177
2020, Dec 22	24.8	179

today's technology. Since in this case we follow a presumably known orbit, several observations during only one night provides enough information, but multiple nights are generally preferred. We stress that taking observations at the first of the possible windows (around February 16, 2002) is useful, but not essential to ensure recovery at subsequent apparitions.

In what follows we envisage a schedule with optical astrometry observations taken on 2002, 2009 and at the two occasions in 2013. Each time we assume three exposures during one night of observations with a formal error of an arc–second in right ascension and half this value in declination. The position of 1998 KY_{26} at the assumed observation time was computed using the nominal force model and a random noise of 0.25 arc–seconds was superimposed. We have checked that the possible sky–plane displacement produced by the Yarkovsky effect is within the quoted observational uncertainties until 2013. In passing, we mention that 1998 KY_{26} comes within 0.12 AU of the Earth in September 2013. Given expected improvements in the radar technology, the asteroid might be even observed with radar at that time; however, we shall neglect this possibility in our considerations.

We have added these assumed observations to the currently available optical and radar observations and performed the same analysis as for the previous asteroids. We have propagated the initial data (state vector and covariance matrix) to the close approach in June 2024, keeping the two–solutions method explained in Sec. 4.1. The 3–σ uncertainty hyper–ellipsoids were then projected onto the radar observables plane, since we assume the possibility of the radar measurements. In this case we considered up to four days before and after the close approach of the nominal orbit. As far as the Yarkovsky model parameters are concerned, we assumed the surface thermal conductivity of 0.1 W/m/K, that appears to us the most likely value in this case, and the ecliptic

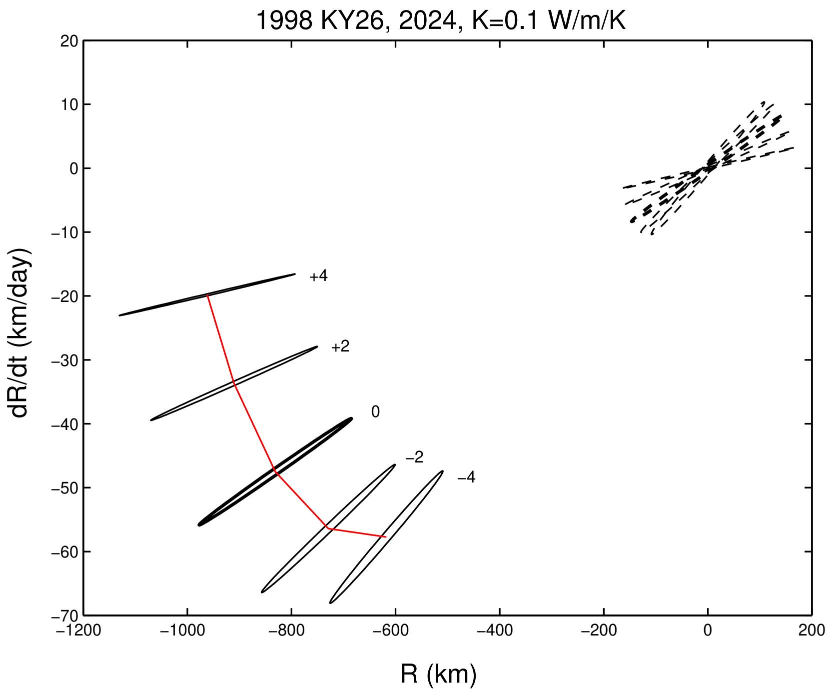

Fig. 17.— Range vs. range–rate plane with 3–σ uncertainty regions at the next close approach of 1998 KY$_{26}$ in June 2024. Notation as in the previous figures. Labels mean days before and after the nominal close approach of the asteroid. The solution assumes optical observations at 2002, 2009 and 2013 (see the text for details). The Yarkovsky orbits (solid lines) assume 0.1 W/m/K for the surface thermal conductivity and the spin axis aligned with the ecliptic pole.

pole orientation of the spin axis of the asteroid. Dependence on both parameters will be discussed below. The results are compared in Fig. 17. We note the statistically very significant separation of the uncertainty regions in the two models, at the level of 17σ. The Yarkovsky perturbation is then not only a surely noticeable phenomenon, but large enough to probe some features of the thermal model of the asteroid. Interestingly enough, the Yarkovsky perturbation is sufficiently large to produce an observable shift of the sky–position of 1998 KY$_{26}$. In Fig. 18 we have projected the 3–σ uncertainty regions onto the sky–plane. As expected, based on the low inclination of the orbit and the nature of the Yarkovsky effect, the difference of the two solutions shows mainly in right ascension.

We recall that we used 0.1 W/m/K for surface conductivity of 1998 KY$_{26}$, but by inspecting the results in Fig. 7 we notice that this does not maximize the effect. Taking the lowest still "reasonable" value of the surface thermal conductivity, notably 0.01 W/m/K, the perturbation would be larger by a factor of about 2.5. However, the orientation of the spin axis of 1998 KY$_{26}$ is probably the principal unknown parameter in our computation. We have used a suggestion by P. Pravec that the axis might not be far from the ecliptic pole, which in fact favors the Yarkovsky

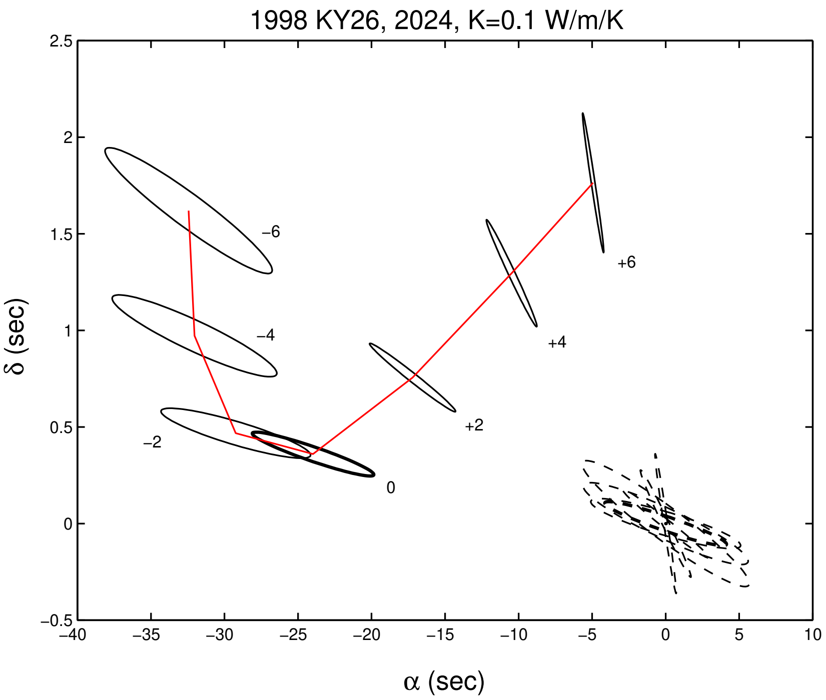

Fig. 18.— The same as in Fig. 17 but projected onto the sky plane parametrized by right ascension (abscissa) and declination (ordinate). Note the different scale of the axes.

perturbation. Since the diurnal variant of the Yarkovsky effect dominates the perturbation we might approximately scale our result by the value $\sin b$ if the ecliptic latitude b of the spin axis is not equal to 90 degrees. A 45 degree latitude would still lead to a Yarkovsky perturbation reduced by a factor of only $1/\sqrt{2} \simeq 0.7$. Moreover, the 2024 close approach might offer photometric observations at different phase than the 1998 observations so that we would get a better constraint of the axis orientation (the intermediate 2002, 2009 and 2013 observations taken at zero phase could also add to this understanding).

We also mention that the first trace of the Yarkovsky perturbation on the orbit of 1998 KY_{26} may already be evident in the December 2020 optical observations (see Table 2). Note that such observations have not been used in the previous analysis so that they can serve as a probe for the Yarkovsky perturbation of the orbit in the same way as the radar data during the 2024 close approach. Figure 19 shows the sky–projected 3–σ uncertainty ellipsoids of the nominal and Yarkovsky–included solutions as before. The polar spin axis of the asteroid and $K = 0.1$ W/m/K surface thermal conductivity are assumed. We note that the Yarkovsky perturbation shows as a slight right ascension offset of about $1.5''$. This value is much smaller than the mean offset in Fig. 18 since at the December 2020 epoch the asteroid is at a distance of 0.47 AU from the Earth while in June 2024 at only 0.03 AU. The difference between Figs. 18 and 19 is well explained by the ratio of the corresponding geocentric distance (note that the four years between the two observations does not significantly increase the Yarkovsky displacement). As a result, the 2020 observation of 1998 KY_{26} might not only help constrain the orbit for the 2024 close approach but might also allow the detection of the Yarkovsky effect on this particular object.

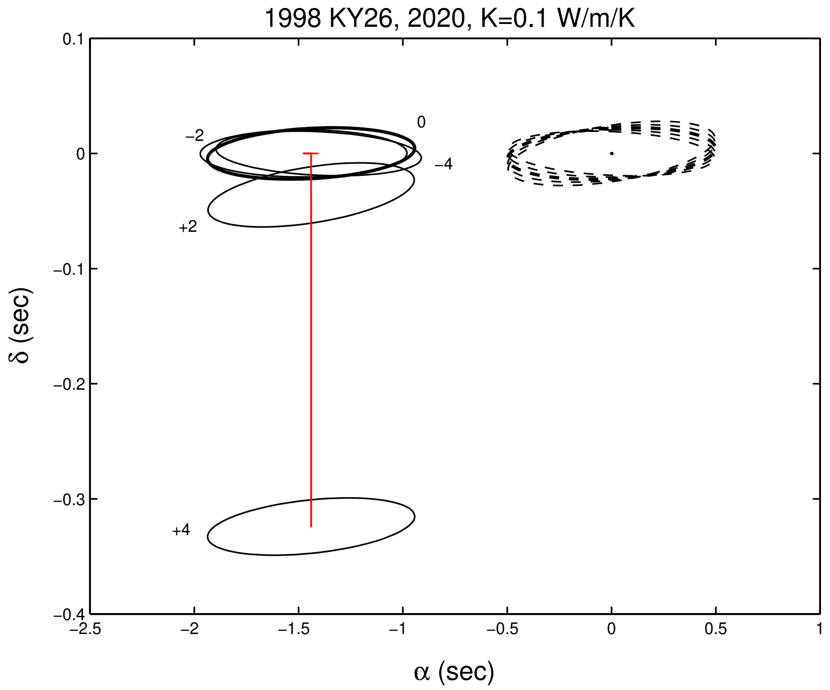

Fig. 19.— The same as in Fig. 18 but for a possible observation of 1998 KY_{26} in December 2020.

4.6. More objects

We have already mentioned that the asteroids discussed in detail above only sample a potentially broader class of objects for which the Yarkovsky perturbation might grow to an observable threshold in the next decades. Toro has been pointed out in this respect. We finish this section by listing a few additional noteworthy asteroids.

- 3908 Nyx has been observed by radar in September and November 1988 and will approach the Earth in November 2004. All physical data necessary for modeling the Yarkovsky force are available (Drummond and Wisniewski 1990). The estimated radius of this asteroid ranges from 0.5–1.1 km, depending on the assumed albedo, which implies a non-negligible semimajor axis drift by the Yarkovsky effect.

- 4769 Castalia has radar observations in August 1989, with the next close approaches in August

2012 and 2023, and in April 2027. Shape and rotation models were resolved from the 1989 radar campaign (Hudson *et al.* 1997).

- 1990 OS was observed with radar in August 1990, with the next close approaches in November 2003 and July 2027. This is a particularly small object with radius of 150–340 meters that may exhibit a fast Yarkovsky drift of the semimajor axis. Unfortunately, no information about the rotation period and orientation of the spin axis is currently available.

- 7341 1991 VK has a single radar apparition in January 1997. Of particular interest is the fact that this asteroid returns to have a close approach to the Earth every 5 years, and that the next one is in January 2002. The regular observability of the orbit by radar offers a unique chance to obtain a very precise orbit for this object. Depending on the assumed albedo, the radius is in the range 0.7–1.6 km, still a promisingly small value for detection of the Yarkovsky effect. The rotation period is known precisely enough (Pravec *et al.* 1998), but we need to determine the spin axis orientation.

- 1996 JG has been observed by radar in May 1996, and the next possibility appears in November 2003. An appreciably large Yarkovsky perturbation may be expected due to the small size of this asteroid (only 150–350 meters in radius). The echo bandwidth of the 1996 radar observations suggest a couple of rotation cycles per day. No information about the spin axis orientation is known.

- 1999 FN19 was observed with radar in April 1999, shortly after its discovery. The next radar observing opportunity is is 2018. Its small size, in the range 100–200 meters, makes it an excellent candidate for revealing the Yarkovsky effect at that time. It is worth noting that its recovery in 2018 would be improbable without the 1999 radar astrometry.

5. Conclusions

Though the problem of high orbital eccentricity has been successfully dealt with in this paper, there remain a number of challenging problems for future work. Most importantly, in all computations of this paper we have applied a thermophysical model based on a spherical body. For each of the asteroids we used a sphere with properly adjusted radius (so that the mass of the asteroid is equal to the mass of its spherical approximation). However, the actual shape of these small objects is typically highly irregular and at the lowest level of approximation they should be represented by a triaxial ellipsoid rather than by a sphere. Developing the asteroid–tailored thermophysical models for each of the cases would be valuable for refining results reported in this paper. Moreover, such models should take into account the complex evolution of the asteroid spin axis, in contrast to the assumption of a constant orientation used throughout this work.

In light of the previous discussion we may say that already in the next decade the orbit determination models of near–Earth asteroids will necessarily require that the Yarkovsky effect be modeled. However, we note that the conclusions of this paper may go even beyond this level. Acquiring radar observational data for very small near–Earth asteroids, of which the object 1998 KY_{26} may be a first example, can leave us in a position to study the Yarkovsky effect in some detail. The size of the orbital perturbation may allow us to not only detect the effect itself, but also to constrain some of the model parameters, in particular the surface thermal conductivity. These parameters might, in turn, indicate the physical character of the object's surface, thus complementing other types of observations.

Acknowledgements. We thank G. Valsecchi for helpful discussions that initiated our work on this project and the other members of the OrbFit Consortium (M. Carpino, Z. Knežević) for their contributions to the software system, which has been used in all the orbit determinations and observation predictions of this paper. We are grateful to P. Chodas for assisting us with the correct interpretation of the radar data, and to S. Ostro for numerous suggestions that helped to shape the final manuscript. We started this work with P. Farinella, whose suggestions and contributions were particularly valuable, but unfortunately he could not join us in the conclusive part of this research because of his health problems and premature death.

REFERENCES

Bottke, W.F., D.P. Rubincam, and J.A. Burns 2000. Dynamical evolution of main belt meteoroids: Numerical simulations incorporating planetary perturbations and Yarkovsky thermal forces. *Icarus*, in press.

Brouwer, D., and G.M. Clemence 1961. *Methods of Celestial Mechanics.* Academic Press, New York.

Brož, M., D. Vokrouhlický, and P. Farinella 2000. Interaction of the Yarkovsky–driven orbits of meteoroids and their precursors with the weak resonances in the main belt. *Icarus*, to be submitted.

Casotto, S. 1992. Position and velocity perturbations in the orbital frame in terms of classical element perturbations. *Celest. Mech. Dyn. Astron.* **55**, 209–222.

De Angelis, G. 1995. Asteroid spin, pole and shape determinations. *Planet. Sp. Sci.* **43**, 649–682.

Drummond, J.D., and W.Z. Wisniewski 1990. The rotational poles and shapes of 1580 Betulia and 3908 (1980PA) from one apparition. *Icarus* **83**, 349–359.

Farinella, P., and D. Vokrouhlický 1999. Semimajor axis mobility of asteroidal fragments. *Science* **283**, 1507–1510.

Farinella, P., D. Vokrouhlický, and W.K. Hartmann 1998. Meteorite delivery via Yarkovsky orbital drift. *Icarus* **132**, 378–387.

Glegg, P.E., J.A. Bastin, and A.E. Gear 1966. Heat transfer in lunar rock. *Mon. Not. Roy. Astr. Soc.* **133**, 63–66.

Goldstein, R.M. 1969. Radar observations of Icarus. *Science* **162**, 903–904.

Graf, T., and K. Marti 1995. Collisional history of H chondrites. *J. Geophys. Res.* **100**, 21–47.

Harris, A.W. 1998. A thermal model for near–Earth asteroids. *Icarus* **131**, 291–301.

Hartmann, W.K., P. Farinella, D. Vokrouhlický, S.J. Weidenschilling, A. Morbidelli, F. Marzari, D.R. Davis, and E. Ryan 1999. Reviewing the Yarkovsky effect: New light on the delivery of stones and irons from the asteroid belt. *Meterit. Space Sci.* **34**, A161–A168.

Herzog, G.F., S. Vogt, A. Albrecht, S. Xue, D. Fink, J. Klein, R. Middleton, H. Weber, and L. Schultz 1997. Complex exposure histories for meteorites with "short" exposure ages. *Meteor. Planet. Sci.* **32**, 413–422.

Hicks, M.D., M.S. Hanner, D.L. Rabinowitz, B.J. Burrati, T.J. Hayward, U. Fink, and W. Grundy 1999. 6489 Golevka revisited: New evidence for a pyroxene-rich near-Earth asteroid. *Bull. Am. Astr. Soc.* **31**, 1072.

Hudson, R.S., S.J. Ostro and A.W. Harris 1997. Constraints on spin state and Hapke parameters of asteroid 4769 Castalia using lightcurves and a radar-derived shape model. *Icarus* **130**, 165–176.

Hudson, R.S. and 26 colleagues 2000. Radar Observations and Physical Modeling of Asteroid 6489 Golevka. *Icarus*, submitted.

Lieske, J.H., and G.W. Null 1969. Icarus and the determination of astronomical constants. *Astron. J.* **74**, 297–307.

Mahapatra, P.R., S.J. Ostro, L.A.M. Benner, K.D. Rosema, R.F Jurgens, R. Winkler, R. Rose, J.D. Giorgini, D.K. Yeomans, and M. Slade 1999. Recent radar observations of asteroid 1566 Icarus. *Planet. Space Sci.* **47**, 987–995.

Magnusson, P. and 46 colleagues 1997. Photometric observations and modeling of asteroid 1620 Geographos. *Icarus* **123**, 227–244.

Milani, A. 1999. The asteroid identification problem I. Recovery of lost asteroids. *Icarus* **137**, 269–292.

Mottola, S. and 28 colleagues 1997. Physical model of near-Earth asteroid 6489 Golevka (1991 JX) from optical and infrared observations. *Astron. J.* **114**, 1234–1245.

Müller, T.G., J.S.V. Lagerros, and J.A.D.L. Blommaert 1999. Fundamental properties and thermophysical modelling of asteroids after ISO. *Bull. Am. Astr. Soc.* **31**, 1075.

Ostro, S.J. and 11 colleagues 1995. Extreme elongation of asteroid 1620 Geographos from radar images. *Nature* **375**, 474–476.

Ostro, S.J. and 12 colleagues 1996. Radar observations of asteroids 1620 Geographos. *Icarus* **121**, 46–66.

Ostro, S.J. and 15 colleagues 1999a. Asteroids 4179 Toutatis: 1996 radar observations. *Icarus* **137**, 122–139.

Ostro, S.J. and 19 colleagues 1999b. Radar and optical observations of asteroid 1998 KY26. *Science* **285**, 557–559.

Pravec, P., M. Wolf, and L. Šarounová 1998. Lightcurves of 26 near-Earth asteroids. *Icarus* **136**, 124–153.

Rubincam, D.P. 1987. LAGEOS orbit decay due to infrared radiation from Earth. *J. Geophys. Res.* **92**, 1287–1294.

Rubincam, D.P. 1995. Asteroid orbit evolution due to thermal drag. *J. Geophys. Res.* **100**, 1585–1594.

Rubincam, D.P. 1998. Yarkovsky thermal drag on small asteroids and Mars-Earth delivery. *J. Geophys. Res.* **103**, 1725–1732.

Shapiro, I.I., W.B. Smith, M.E. Ash, and S. Herrick 1971. General relativity and the orbit of Icarus. *Astron. J.* **76**, 588–606.

Sitarski, G. 1992. On the relativistic motion of (1566) Icarus. *Astron. J.* **104**, 1226–1229.

Sitarski, G. 1998. Motion of the minor planet 4179 Toutatis: Can we predict its collision with the Earth? *Acta Astron.* **48**, 547–561.

Spitale, J., and R. Greenberg 1999. Numerical investigation of the Yarkovsky effect: Mutiny on the high e's. *Bull. Am. Astr. Soc.* **31**, 1112.

Spitale, J., and R. Greenberg 2000. Numerical evaluation of the general Yarkovsky effect: Effects on semimajor axis. *Icarus*, submitted.

Veeder, G.J., M.S. Hanner, D.L. Matson, E.F. Tedesco, L.A. Lebofsky, and A.T. Tokunaga 1989. Radiometric of near-Earth asteroids. *Astron. J.* **97**, 1211–1219.

Vokrouhlický, D. 1998a. Diurnal Yarkovsky effect as a source of mobility of meter-sized asteroidal fragments: I. Linear theory. *Astron. Astrophys.* **335**, 1093–1100.

Vokrouhlický, D. 1998b. Diurnal Yarkovsky effect as a source of mobility of meter-sized asteroidal fragments: II. Non-Sphericity Effects. *Astron. Astrophys.* **338**, 353–363.

Vokrouhlický, D. 1999. A complete linear model for the Yarkovsky thermal force on spherical asteroid fragments. *Astron. Astrophys.* **344**, 362–366.

Vokrouhlický, D., and M. Brož 1999. An improved model of the seasonal Yarkovsky force for the regolith-covered asteroid fragments. *Astron. Astrophys.* **350**, 1079–1084.

Vokrouhlický, D., and P. Farinella 1998. The Yarkovsky seasonal effect on asteroidal fragments: A nonlinearized theory for the plane-parallel case. *Astron. J.* **116**, 2032–2041.

Vokrouhlický, D., and P. Farinella 1999. The Yarkovsky seasonal effect on asteroidal fragments: A non–linearized theory for spherical bodies. *Astron. J.*, **118**, 3049–3060.

Vokrouhlický, D., and P. Farinella 2000. Delivery of stony meteorites from the asteroid belt. *Nature*, submitted.

Vokrouhlický, D., M. Brož, P. Farinella, and Z. Knežević 2000. Yarkovsky–driven leakage of Koronis family members: I. The case of 2953 Vysheslavia. *Icarus*, submitted.

Wechsler, A.E., P.E. Glaser, A.D. Little, and J.A. Fountain 1972. Thermal properties of granulated materials, in: *Thermal Characteristics of the Moon* (J.W. Lucas, Ed.), pp. 215–241. MIT Press, Cambridge.

Wesselink, A.J. 1948. Heat conductivity and nature of the lunar surface material. *Bull. Astr. Inst. Nether.* **10**, 351–363.

Yeomans, D. 1991. A comet among the near–Earth asteroids? *Astron. J.* **101**, 1920–1928.

Yeomans, D. 1992. Erratum: "A comet among the near-Earth asteroids?" *Astron. J.* **104**, 1266.

Yeomans, D., P.W. Chodas, M.S. Keesey, S.J. Ostro, J.F. Chandler, and I.I. Shapiro 1992. Asteroid and comet orbits using radar data. *Astron. J.* **103**, 303–317.

Yomogida, K., and T. Matsui 1983. Physical properties of ordinary chondrites. *J. Geophys. Res.* **88**, 9513–9533.

Zaitsev, A.L. and 24 colleagues 1997. Intercontinental bistatic radar observations of 6489 Golevka (1991 JX). *Planet. Space Sci.* **45**, 771–778.

This preprint was prepared with the AAS LaTeX macros v5.0.